THE GEOLOGICAL SOCIETY OF AMERICA®

Oxygen isotopic investigation of silicic magmatism in the Stillwater caldera complex, Nevada: Generation of large-volume, low-$\delta^{18}O$ rhyolitic tuffs and assessment of their regional context in the Great Basin of the western United States

Kathryn E. Watts[1,†], David A. John[1], Joseph P. Colgan[2], Christopher D. Henry[3], Ilya N. Bindeman[4], and John W. Valley[5]

[1]*U.S. Geological Survey, Menlo Park, California 94025, USA*
[2]*U.S. Geological Survey, Denver, Colorado 80225, USA*
[3]*Nevada Bureau of Mines and Geology, Reno, Nevada 89557, USA*
[4]*Department of Earth Sciences, University of Oregon, Eugene, Oregon 97403, USA*
[5]*Department of Geoscience, University of Wisconsin–Madison, Madison, Wisconsin 53706, USA*

ABSTRACT

Successive caldera-forming eruptions from ca. 30 to 25 Ma generated a large nested caldera complex in western Nevada that was subsequently dissected by Basin and Range extension, providing extraordinary cross-sectional views through diverse volcanic and plutonic rocks. A high-resolution oxygen isotopic study was conducted on units that represent all major parts of the Job Canyon, Louderback Mountains, Poco Canyon, and Elevenmile Canyon caldera cycles (29.2–25.1 Ma), and several Cretaceous plutons that flank the Stillwater caldera complex. We provide new oxygen and strontium isotope data for 12 additional caldera centers in the Great Basin, which are synthesized with >150 published oxygen and strontium isotope analyses for regional Mesozoic basement rocks. Stillwater zircons span a large isotopic range ($\delta^{18}O_{zircon}$ of 3.6‰–8.2‰), and all caldera cycles possess low-$\delta^{18}O$ zircons. In some cases, they are a small proportion of the total populations, and in others, they dominate, such as in the low-$\delta^{18}O$ rhyolitic tuffs of Job Canyon and Poco Canyon ($\delta^{18}O_{zircon}$ = 4.0‰–4.3‰; $\delta^{18}O_{magma}$ = 5.5‰–6‰). These are the first low-$\delta^{18}O$ rhyolites documented in middle Cenozoic calderas of the Great Basin, adding to the global occurrence of these important magma types that fingerprint recycling of shallow crust altered by low-$\delta^{18}O$ meteoric waters. The appearance of low-$\delta^{18}O$ rhyolites in the Stillwater caldera complex is overprinted on a Great Basin–wide trend of miogeoclinal sediment contribution to silicic magmas that elevates $\delta^{18}O$ compositions, making identification of ^{18}O depletions difficult. Though not a nominally low-$\delta^{18}O$ rhyolite, the tuff of Elevenmile Canyon possesses both low-$\delta^{18}O$ and high-$\delta^{18}O$ zircon cores that are overgrown by homogenized zircon rims that approximate the bulk zircon average, pointing to batch assembly of isotopically diverse upper crustal melts to generate one of the most voluminous (2500–5000 km^3) tuff eruptions in the Great Basin. Despite overlapping in space and time, each caldera-forming cycle of the Stillwater complex has a unique oxygen isotope record as retained in single zircons. Most plutons that were spatially and temporally coincident with calderas have isotopic compositions that diverge from the caldera-forming tuffs and cannot be their cogenetic remnants.

INTRODUCTION

During the middle Cenozoic, tens of thousands of cubic kilometers of silicic magma erupted from dozens of calderas that span across Nevada in a broad northwest to southeast belt (Fig. 1; Best et al., 2013a). This ignimbrite flare-up may have been related to steepening, or roll-back, of the subducting Farallon plate beneath the western edge of North America (Coney and Reynolds, 1977; Coney, 1978; Humphreys, 1995). Although most calderas occur within intact crustal blocks, some were dissected and significantly tilted by Basin and Range extension during the late Cenozoic, providing valuable windows into the volcanic and plutonic processes that underpinned them, and perhaps by analogue, the life spans and eruptive potential of modern-day caldera volcanoes.

Caldera exposures are exemplified by the Stillwater–Clan Alpine complex in western Nevada (Figs. 1–2; abbreviated here and elsewhere as the Stillwater caldera complex). The western margin of the complex in the Stillwater Range is steeply tilted, exposing an ~10 km depth section through the upper crust, including several overlapping calderas and plutons that provide a unique opportunity to elucidate the petrogenesis of large-volume silicic magmas in the Great Basin ignimbrite flare-up. Here, we present the results of a comprehensive oxygen isotopic investigation, with particular emphasis on refractory zircon crystals, which demonstrate significant diversity in Stillwater magmas, including two low-$\delta^{18}O$ rhyolitic tuffs (Job Canyon and Poco Canyon; $\delta^{18}O_{magma}$ = 5.5‰–6‰). To our knowledge, these are the first low-$\delta^{18}O$ rhyolites described in the Great Basin ignimbrite flare-up. The low-$\delta^{18}O$ Ammonia Tanks Tuff ($\delta^{18}O_{magma}$ = 5.4‰–6‰) in

†kwatts@usgs.gov

GSA Bulletin; July/August 2019; v. 131; no. 7/8; p. 1133–1156; https://doi.org/10.1130/B35021.1; 12 figures; 4 tables; Data Repository item 2019060; published online 14 February 2019.

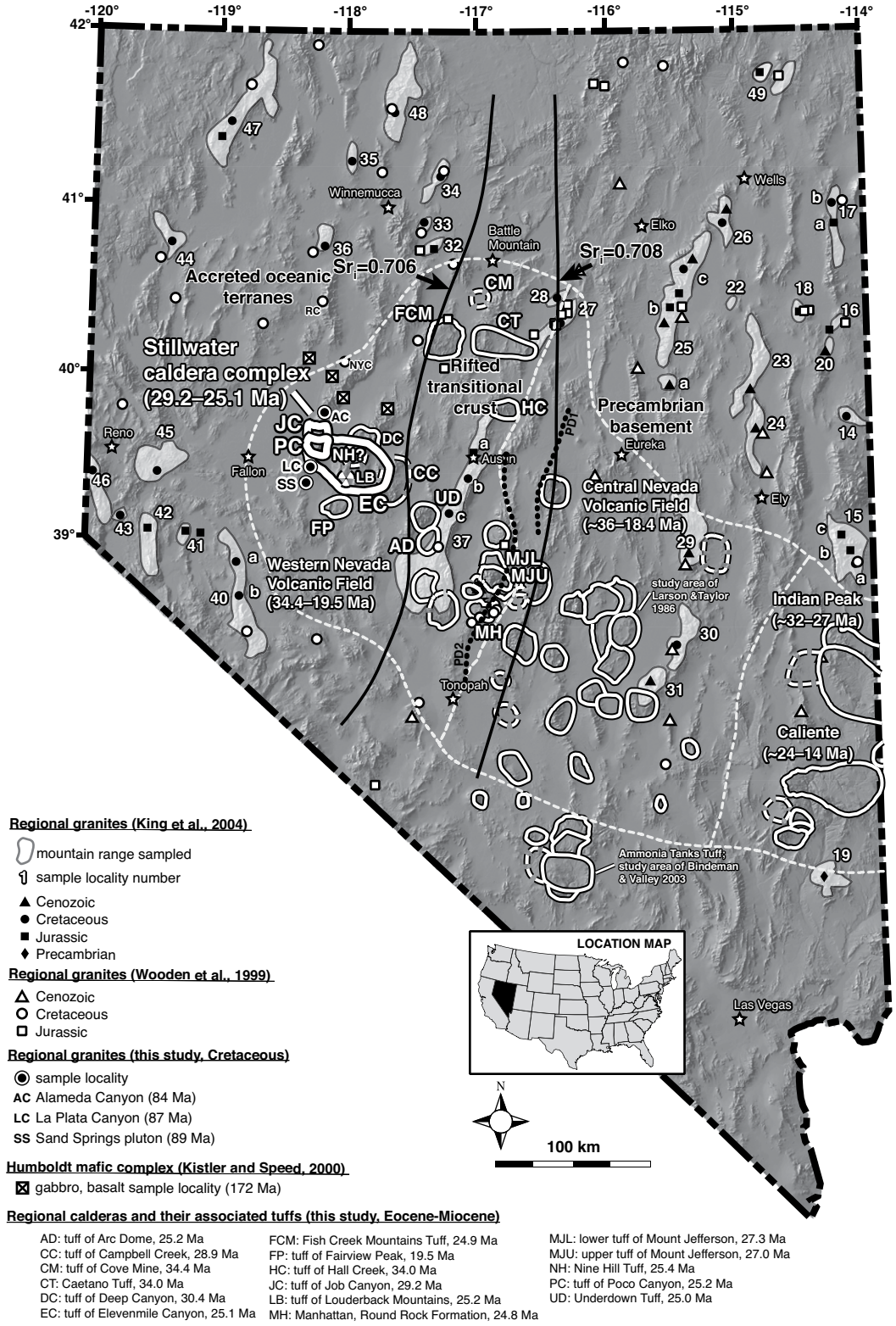

Figure 1. Map showing the location of the Stillwater caldera complex and other middle Cenozoic calderas in the Great Basin, Nevada. Calderas are subdivided into the western Nevada, central Nevada, and Indian Peak–Caliente volcanic fields (Best et al., 2013a). Dashed pale-gray lines show the boundaries between volcanic fields, black solid lines show the locations of the $^{87}Sr/^{86}Sr_i = 0.706$ and $^{87}Sr/^{86}Sr_i = 0.708$ isopleths (Farmer and DePaolo, 1983), and dotted black lines show the paleodivide boundaries of Henry and John (2013) ("PD1") and Best et al. (2013a) ("PD2"). The mountain ranges sampled by King et al. (2004) are shaded in gray and numbered according to their numbering scheme. Labels and ages for the calderas and granites included in this study are shown in the figure legend. Labels are included for two Cretaceous granite localities to the north of the Stillwater caldera complex, the New York Canyon (NYC) stock and the Rocky Canyon (RC) pluton, which may be pertinent to the basement crustal architecture (see text for detail). Stars show town localities in Nevada.

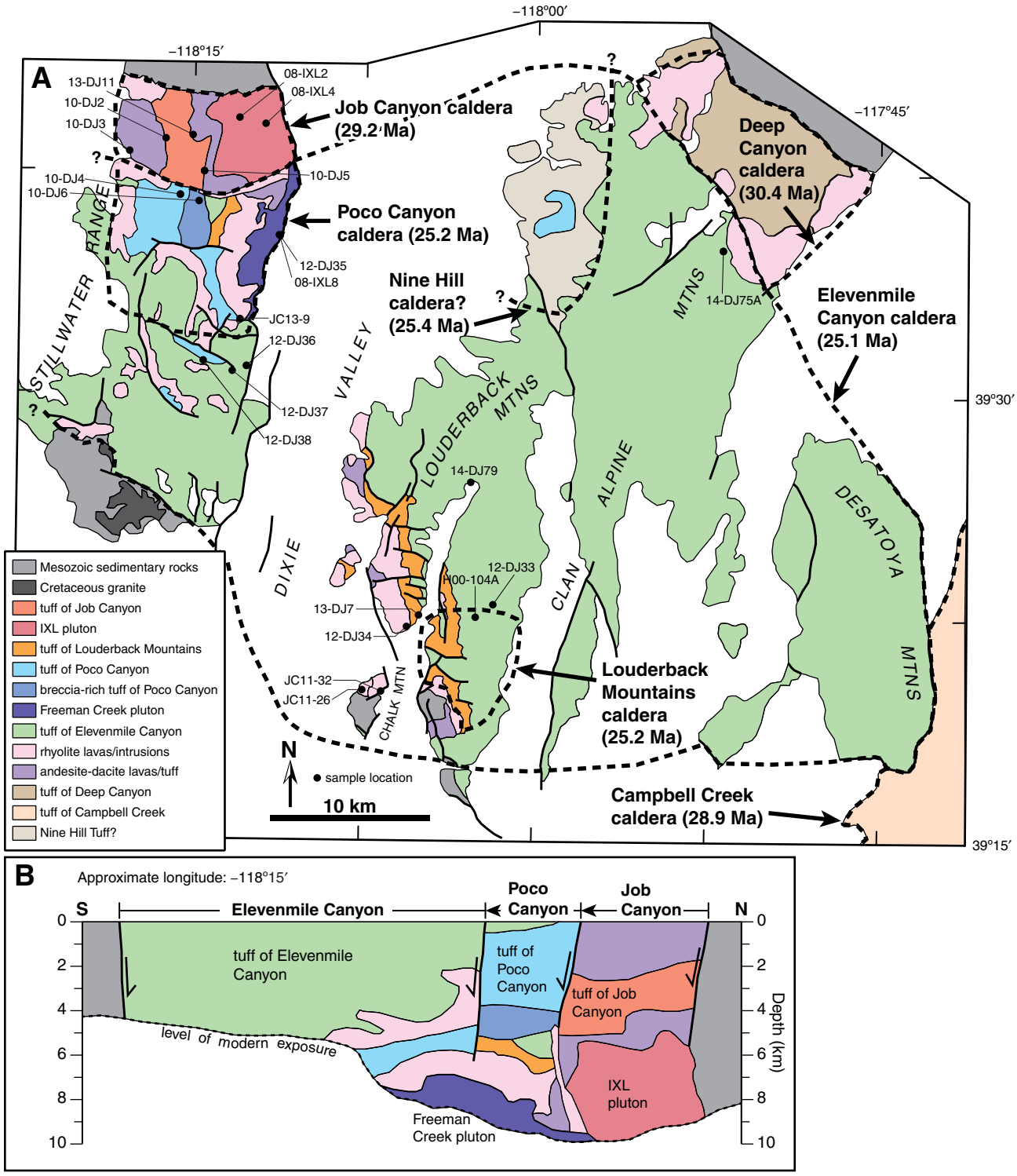

Figure 2. Simplified geologic map and cross section of the Stillwater caldera complex, modified after Colgan et al. (2018). (A) Approximate caldera margins for seven overlapping calderas are shown by the bold dashed lines; thin bold lines show faults, some of which bound the caldera margins. Distributions of Mesozoic basement rocks and rocks of the Stillwater caldera complex are shown by the filled polygons and legend. (B) Pretilt north-south cross section through three overlapping calderas in the Stillwater Range: the Job Canyon, Poco Canyon, and Elevenmile Canyon calderas.

southern Nevada (Fig. 1) was produced during the much younger regime of late Cenozoic Basin and Range extensional tectonics and magmatism (Bindeman and Valley, 2003). Low-$\delta^{18}O$ rhyolites fingerprint hydrothermally altered crustal materials that have exchanged oxygen with low-$\delta^{18}O$ meteoric waters (Taylor, 1986), thus revealing a shallow process of crustal recycling heretofore not recognized in the Great Basin ignimbrite flare-up.

In addition to providing important new constraints on Cenozoic silicic magmatism in the Great Basin, this study adds to the occurrence of low-$\delta^{18}O$ rhyolites worldwide that signify an important part of the geochemical evolution of Earth's continental crust as it interacts with the hydrosphere. Low-$\delta^{18}O$ rhyolites have been documented in huge volumes (>10,000 km^3) to the north of the Great Basin in caldera centers of the Snake River Plain–Yellowstone hotspot track (Hildreth et al., 1984; Bindeman and Valley, 2001; Boroughs et al., 2005; Bindeman et al., 2008; Ellis et al., 2010; Watts et al., 2011, 2012; Drew et al., 2013; Colón et al., 2015; Loewen and Bindeman, 2015; Blum et al., 2016; Troch et al., 2017). Other settings in which they have been documented include present or former rift environments, such as Iceland (Bindeman et al., 2012; Pope et al., 2013) and South Africa (Harris and Erlank, 1992), and modern subduction zone environments such as the Kamchatka Peninsula in Russia (Bindeman et al., 2004; Seligman et al., 2014), the southern Andes in South America (Grunder, 1987), and Crater Lake in the Oregon Cascades (Bacon et al., 1989; Ankney et al., 2017). Despite this ubiquity, the importance of low-$\delta^{18}O$ rhyolites to our understanding of crustal magmatism likely remains underestimated due to the dearth of oxygen isotope data needed to identify them, and the propensity for such shallow rocks to be stripped from the geologic record. Geographic location also has a profound effect on the presence and magnitude of ^{18}O depletion of meteoric waters, and therefore, regardless of tectonic setting and mechanism, the processes associated with low-$\delta^{18}O$ rhyolite genesis may be obscure in many regions, such as in near-equatorial latitudes or arid environments (e.g., Folkes et al., 2013).

The Great Basin, which possesses a world-class endowment of hydrothermally altered and mineralized crustal basement rocks as well as dozens of overlapping caldera centers with hydrothermal alteration (e.g., Best et al., 2013a; Henry and John, 2013), is a prime setting in which low-$\delta^{18}O$ rhyolites would be expected to occur. The Stillwater caldera complex in particular, with caldera-forming tuffs, plutons, and an ancient hydrothermal system exposed to ~10 km depth (John, 1995; John and Pickthorn, 1996), may be a critical locality for evaluating processes of low-$\delta^{18}O$ rhyolite genesis in the Great Basin and worldwide.

GEOLOGIC BACKGROUND

The western margin of the North American continent consists of three major crustal zones in the Great Basin, from Precambrian cratonic basement in eastern Nevada ($^{87}Sr/^{86}Sr_i > 0.708$), to transitional rifted crust and sedimentary rocks of the miogeocline in central Nevada ($^{87}Sr/^{86}Sr_i$ ~0.706–0.708), to accreted oceanic terranes in western Nevada ($^{87}Sr/^{86}Sr_i < 0.706$) (Fig. 1; Farmer and DePaolo, 1983). Tectonic interaction between the continental margin and accreted terranes has resulted in a complex juxtaposition of Paleozoic–Mesozoic lithologic assemblages (cf. Crafford, 2008). Overprinted on this complex basement geology are three major pulses of silicic igneous activity, manifested by Jurassic and Cretaceous granitic plutons that span across the state of Nevada and a broad (>400 km) belt of middle Cenozoic calderas (Fig. 1).

The western Nevada, central Nevada, and Indian Peak–Caliente volcanic fields subdivide the numerous calderas of the middle Cenozoic caldera belt (Fig. 1; Henry and John, 2013; Best et al., 2013b, 2013c). Diameters of individual calderas range from ~10 to 50 km, and volumes of ignimbrites range from ~50 to >1000 km^3, with well over a dozen that can be classified as "supereruptions" (cf. Miller and Wark, 2008). Compositionally, the ignimbrites are diverse, ranging from rhyolitic to trachydacitic (~78–63 wt% SiO_2), and crystal-poor (<15 vol%) to highly crystal-rich (>35 vol%). In areas where Basin and Range extensional faulting has exposed relatively deep (>5 km) cross-sectional views through calderas, voluminous plutons underlie and intrude the caldera stratigraphy (e.g., John, 1995; John et al., 2008). Geochronologic and petrologic studies support a cogenetic origin for at least some of these caldera-forming tuffs and plutons (e.g., Watts et al., 2016).

The Stillwater caldera complex is the westernmost expression of caldera-forming eruptions in the western Nevada volcanic field (Fig. 1). From west to east, the complex spans the Stillwater Range, Louderback Mountains, Clan Alpine Mountains, and Desatoya Mountains (Fig. 2; Colgan et al., 2018). Seven nested calderas were formed in two discrete pulses, with ignimbrite eruptions at ca. 30.4–28.9 Ma and ca. 25.4–25.1 Ma (Fig. 2; Henry and John, 2013; Colgan et al., 2018). In this paper, we present detailed oxygen isotope data for four caldera-forming tuffs and associated lava flows and plutonic rocks, including the tuffs of Job Canyon (ca. 29.2 Ma, >55 km^3), Louderback Mountains (ca. 25.2 Ma, ≤50 km^3?), Poco Canyon (ca. 25.2 Ma, >360 km^3), and Elevenmile Canyon (ca. 25.1 Ma, 2500–5000 km^3). We also provide data for three Late Cretaceous granitic intrusions in the Stillwater Range, the Alameda Canyon (ca. 84 Ma), La Plata Canyon (ca. 87 Ma), and Sand Springs (ca. 89 Ma) plutons (Fig. 1), to test whether they are potential crustal sources for ca. 30–25 Ma Stillwater magmas. Here, we briefly describe each of the studied caldera cycles and note some of the remaining uncertainties. We refer the reader to John (1995), Henry and John (2013), and Colgan et al. (2018) for additional discussion of geologic field relationships and geochronology.

Job Canyon Cycle

The ca. 29–28 Ma Job Canyon caldera consists of sequences of andesite-dacite lavas, breccias, and minor pyroclastic rocks that both underlie and overlie the ~2-km-thick caldera-forming rhyolitic (~71–77 wt% SiO_2) tuff of Job Canyon and associated megabreccia (John, 1995). The volcanic rocks have a total thickness of ~5 km. The ca. 28 Ma IXL pluton (~59–69 wt% SiO_2) intrudes precaldera lavas and Mesozoic metasedimentary rocks.

Louderback Mountains Cycle

The trachydacitic to rhyolitic (~69–76 wt% SiO_2) tuff of Louderback Mountains overlies rhyolite lavas and contains abundant blocks of them where it fills the Louderback Mountains caldera, inferred to exist in the southwestern Clan Alpine Mountains (Colgan et al., 2018). The tuff of Elevenmile Canyon overlies the tuff of Louderback Mountains in this area and in the Louderback Mountains. Altered tuff up to ~1 km thick, which is tentatively correlated with the tuff of Louderback Mountains, overlies rhyolite lavas and underlies rocks of the Poco Canyon caldera in the Stillwater Range (Colgan et al., 2018).

Poco Canyon Cycle

The Poco Canyon caldera system consists of two (lower and upper) cooling units of abundantly porphyritic (~35–45 vol% crystallinity) and rhyolitic (~71–77 wt% SiO_2) tuff of Poco Canyon. Sedimentary rocks and up to ~2 km of crystal-poor rhyolite tuff, which contains abundant mesobreccia and megabreccia blocks of flow-banded rhyolite and the lower crystal-rich rhyolite tuffs separate the two cooling units (John, 1995). The upper cooling unit and underlying breccia-rich tuff total ~4.5 km in thickness. Outflow tuff from the caldera extends

>150 km west and ~60 km east of the caldera (John, 1995). The caldera is underlain by altered, sparsely porphyritic, flow-banded rhyolite lava flows, domes, and intrusive rocks as much as ~1.5 km thick that are locally intercalated with and overlain by silicic welded tuffs, andesites, and minor sedimentary rocks.

Elevenmile Canyon Cycle

Rocks of the Elevenmile Canyon caldera overlie the Poco Canyon and Louderback Mountains calderas, outflow tuff of Poco Canyon, and sparsely porphyritic flow-banded rhyolite lava flows, domes, and intrusive rocks. The trachydacitic to rhyolitic (~65–77 wt% SiO_2) tuff of Elevenmile Canyon is up to ~5 km thick in the Stillwater Range and ~3–4 km thick in the southern Clan Alpine Mountains. Outflow tuff extends ~60 km to the east and ~125 km to the west (Henry and John, 2013).

Circa 25 Ma Intrusive Rocks

The Poco Canyon and Elevenmile Canyon calderas in the Stillwater Range are underlain and possibly intruded by the ca. 25 Ma Freeman Creek pluton, which consists of an older granodiorite (~65–67 wt% SiO_2) phase and a younger granite (~72–77 wt% SiO_2) phase. Where exposed, the Freeman Creek pluton intrudes rhyolite lavas and undated volcanic rocks that underlie the Poco Canyon and Elevenmile Canyon calderas; it does not directly intrude the tuffs, although it may do so elsewhere in the subsurface. An ~7-km-long composite granite and rhyolite porphyry dike intrudes the IXL pluton, separating the Job Canyon and Poco Canyon calderas (John, 1995). At Chalk Mountain, rhyolite porphyry and granodiorite plutons (ca. 25 Ma) underlie the Louderback Mountains and Elevenmile Canyon calderas (Colgan et al., 2018). Where exposed, the granodiorite intrudes Mesozoic dolomite, but the area between Chalk Mountain and exposures of the Elevenmile Canyon caldera is covered by alluvium and it is not known if it directly intrudes the intracaldera tuff.

SAMPLES AND METHODS

Oxygen isotope data were collected for 16 caldera centers in the western Nevada volcanic field (labeled in Fig. 1; tabulated in Table 1). Data collected for the Stillwater complex represent four caldera cycles (Job Canyon, Louderback Mountains, Poco Canyon, and Elevenmile Canyon) and three Cretaceous granitic plutons (Alameda Canyon, La Plata Canyon, and Sand Springs). The University of Oregon Stable Isotope Laboratory was used to analyze a variety of mineral phases using the established protocols of Bindeman (2008) for CO_2-laser fluorination. Refractory quartz (single to several crystals per analysis) and bulk zircon were the primary targets, with additional analyses of sanidine, plagioclase, and biotite. Minerals were analyzed in 1.5–2.5 mg aliquots under vacuum with a CO_2 laser and BrF_5 reagent to liberate O_2 gas, which was then purified with a mercury diffusion pump to remove traces of fluorine gas, and converted to CO_2 in a platinum-graphite converter. For reactive sanidine, an airlock chamber was used between analyses to prevent reaction of grains with BrF_5 prior to lasing. A Thermo Finnigan MAT 253 mass spectrometer was used to analyze the oxygen isotopic composition of the CO_2 gas, and $\delta^{18}O$ values are reported relative to Vienna standard mean ocean water (VSMOW). A University of Oregon garnet standard (UOG; $\delta^{18}O$ = 6.52‰, VSMOW) was used to correct $\delta^{18}O$ values in unknowns; UOG analyses ranged from –0.1‰ to –0.6‰ relative to the empirical standard value and had an external reproducibility (2 standard deviations) of 0.1‰–0.2‰. The UOG standard is calibrated to the University of Wisconsin garnet standard (UWG-2; $\delta^{18}O$ = 5.80‰, VSMOW).

Strontium isotope whole-rock data were collected for a subset of the regional caldera centers for which oxygen isotope data were acquired. Combined with published strontium isotope data, these total nine calderas. We have strontium isotope data for three of the four caldera cycles investigated in the Stillwater caldera complex (Job Canyon, Poco Canyon, and Elevenmile Canyon) and the three Cretaceous granitic plutons (Alameda Canyon, La Plata Canyon, and Sand Springs). Whole-rock powders were analyzed for their strontium isotope compositions using a ThermoFinnigan TRITON thermal ionization multicollector mass spectrometer at Carleton University in Ottawa, Canada. Strontium isotopic ratios were corrected for radiogenic ingrowth using published $^{40}Ar/^{39}Ar$ ages, or when not available, $^{206}Pb/^{238}U$ ages (Table 1). Previously published strontium isotope data were corrected for the most up-to-date age data tabulated in Table 1.

Secondary ion mass spectrometry (SIMS) oxygen isotope data were collected for single zircon crystals from 22 samples that represent all major units of the Job Canyon, Poco Canyon, Elevenmile Canyon, and Louderback Mountains caldera cycles, and one sample of the Cretaceous Sand Springs pluton. Prior to SIMS analysis, zircons were separated from crushed whole rocks using a water table, Frantz magnetic separator, and heavy liquids; handpicked under a binocular microscope; mounted in epoxy rounds within a 10 mm diameter in the center of each mount; and ground down to expose the approximate midsections of grain interiors. Zircon standards (KIM-5, R33, MADDER) were included in the center of each mount. A Tescan VEGA3 scanning electron microscope (SEM) at the U.S. Geological Survey (USGS) Menlo Park microanalytical facility was used to map zircon crystals using backscattered electrons (BSE) and cathodoluminescence (CL) to document internal textures and enable precise targeting of core, interior, and rim domains.

Oxygen isotope ratios were analyzed in situ at the WiscSIMS Laboratory at the University of Wisconsin, Madison, using a CAMECA ims 1280 ion microprobe. The WiscSIMS ion microprobe was operated with a $^{133}Cs^+$ beam current of ~2 nA, accelerating potential of 10 kV (20 kV impact energy), and tuned to an ~15 µm ion beam spot diameter (~1 µm deep) on the sample (Kita et al., 2009; Valley and Kita, 2009). Secondary ions of $^{16}O^-$, $^{16}OH^-$, and $^{18}O^-$ were analyzed simultaneously using three Faraday cup detectors. The ion yield for ^{16}O was ~1.4 Gcps/nA. Ratios of $^{16}OH/^{16}O$ were background corrected by comparison to the nominally anhydrous KIM-5 zircon (Wang et al., 2014). Analyses of KIM-5 zircon ($\delta^{18}O$ = 5.09‰, VSMOW; Valley, 2003) bracketed each set of unknowns, with ~4–5 KIM-5 analyses before and after each set of ~15 unknown spots. Values of instrumental mass fractionation based on KIM-5 varied from –1.2‰ to –0.3‰, and the external reproducibility (2 standard deviations) during the analytical session ranged from 0.1‰ to 0.4‰, averaging 0.2‰.

A subset of zircons analyzed for oxygen isotopes using the WiscSIMS ion microprobe was analyzed for $^{206}Pb/^{238}U$ ages and trace elements using a sensitive high-resolution ion microprobe with reverse geometry (SHRIMP-RG) cooperated by the USGS and Stanford University. Zircon mounts were re-imaged by SEM after SIMS analysis to evaluate each analytical spot and to map their precise locations. After polishing away the WiscSIMS pits, the grain domains just beneath each SIMS $\delta^{18}O$ spot were analyzed with the SHRIMP-RG, using a slightly larger diameter ion beam (~20 µm). Zircon U-Pb ages were standardized against R33 (419.3 Ma; Black et al., 2004) and trace elements against MAD-green zircon (Barth and Wooden, 2010). For a full description of the SHRIMP-RG analytical methods used, see Colgan et al. (2018).

Hornblende geochemistry was determined by electron microprobe for the tuff of Elevenmile Canyon in order to constrain the crystallization pressures of Stillwater magmas; hornblende is either absent or highly altered in tuffs of the other major caldera-forming cycles in the Stillwater caldera complex. Polished thin

TABLE 1. OXYGEN AND STRONTIUM ISOTOPE AND AGE DATA FOR CALDERA-FORMING TUFFS AND BASEMENT SAMPLES IN THE WESTERN NEVADA VOLCANIC FIELD

Caldera	Type	Unit	Map ID	Sample(s)	Latitude (°N)	Longitude (°W)	$^{40}Ar/^{39}Ar$ age (Ma)	$^{206}Pb/^{238}U$ age (Ma)	$\delta^{18}O$ average (‰, VSMOW)		Magma† (calc.)	$^{87}Sr/^{86}Sr_i$
									Quartz	Zircon		
Caetano	Single	Caetano Tuff	CT	Many, see Watts et el. (2016)	40.16	–116.82	34.00 ± 0.03 (14)	34.23–34.46 ± 0.2–0.3 (169)	10.7 ± 0.3 (25)	8.7 ± 0.3 (74)	10.2–10.3	0.7068–0.7072
Hall Creek	Single	Tuff of Hall Creek	HC	H11-167, H11-22	39.77	–116.82	33.92 ± 0.02 (4)	34.06 ± 0.40 (23)	10.4 ± 0.3 (4)	–	10.0	–
Cove Mine	Single	Tuff of Cove Mine	CM	H03-87, 05-DJ-8, 06-DJ-13	40.45	*–117.02*	34.44 ± 0.01 (4)	–	10.1 ± 0.4 (7)	–	9.7	0.7067
Fish Creek Mountains	Single	Fish Creek Mountains Tuff	FCM	FCM-2, FCM-5	40.19	–117.28	24.91 ± 0.03 (3)	25.02 ± 0.38 (6)	9.1 ± 0.2 (5)	–	8.7	0.7058–0.7061
Mount Jefferson	Nested	Lower tuff of Mount Jefferson	MJL	H94-28	38.77	–116.90	27.25 ± 0.04 (17)	–	9.7 ± 0.1 (2)	–	9.3	–
Mount Jefferson	Nested	Upper tuff of Mount Jefferson	MJU	H94-4	38.77	–116.90	27.01 ± 0.05 (4)	–	8.9 ± 0.2 (2)	–	8.5	–
Manhattan	Nested?	Diamond King Formation	MH	H94-43	38.58	–117.03	24.66 ± 0.07 (1)	–	8.4 ± 0.1 (2)	–	8.0	–
Arc Dome	Single	Tuff of Arc Dome	AD	17-AD-1	39.00	–117.42	25.15 ± 0.02 (5)	–	8.8 ± 0.3 (2)	–	8.4	–
Underdown	Single	Underdown Tuff	UD	JC13-5	39.14	–117.44	24.91 ± 0.05 (4)	25.32 ± 0.21 (21)	9.0 ± 0.1 (2)	–	8.6	–
Campbell Creek	Nested?	Tuff of Campbell Creek	CC	H02-24	39.36	–117.68	28.94 ± 0.06 (20)	28.94 ± 0.31 (24)	8.8 ± 0.5 (2)	–	8.4	0.7060
Nine Hill	Nested?	Nine Hill Tuff	NH	H03-138	39.50	*–117.94*	25.38 ± 0.08 (12)	–	8.6 ± 0.1 (2)	–	8.2	0.7054
Fairview Peak	Single	Tuff of Fairview Peak	FP	H93-58	39.20	–118.09	19.48 ± 0.02 (3)	19.65 ± 0.22 (21)	7.9 ± 0.2 (2)	–	7.5	0.7050
Elevenmile Canyon	Nested	Tuff of Elevenmile Canyon	EC	Many, see Table 2	39.44	–117.98	25.11 ± 0.03 (28)	25.00–25.82 ± 0.2–0.3 (113)	7.9 ± 0.3 (7)	5.9–6.1 ± 0.1–0.5 (73/112)*	7.4–7.6	0.7051–0.7054
Poco Canyon	Nested	Tuff of Poco Canyon	PC	Many, see Table 2	39.56	–118.25	25.27 ± 0.03 (8)	25.60–25.99 ± 0.2–0.3 (48)	6.5 ± 0.3 (4)	4.0–4.3 ± 0.2 (59/71) *	5.5–5.8	0.7049–0.7055
Louderback Mountains	Nested	Tuff of Louderback Mountains	LB	13-DJ-7, see Table 2	39.39	*–118.00*	25.20 ± 0.02 (2)	25.29–25.78 ± 0.3–0.5 (38)	–	7.1–7.2 ± 0.1–0.2 (17/28)*	8.6–8.7	–
Job Canyon	Nested	Tuff of Job Canyon	JC	10-DJ-2, see Table 2	39.63	–118.26	–	29.25 ± 0.5 (17)	–	4.5 ± 0.3 (19/20)*	6.0	0.7052–0.7057
Basement locality												
Alameda Canyon	–	Alameda Canyon pluton	AC	JC11-25, 16-DJ-31	39.72	–118.20	–	83.92 ± 0.83 (11)	11.5 ± 0.1 (3)	–	11.1	0.7050
La Plata Canyon	–	La Plata Canyon pluton	LC	JC09-LC4, 16-DJ-34	39.43	–118.30	–	87.25 ± 0.50 (12)	10.4 ± 0.1 (3)	–	10.0	0.7051
Sand Springs	–	Sand Springs pluton	SS	JC11-27, 16-DJ-38	39.33	–118.33	–	88.6 ± 3.1 (13)	9.8 ± 0.2 (3)	6.6 ± 0.2 (20)	8.1–9.4	0.7043–0.7047

Note: Latitude and longitude are the approximate centers of individual calderas. *Italics* indicate uncertain caldera location. $^{40}Ar/^{39}Ar$ sanidine ages were compiled from John et al. (2008), Henry and John (2013), Watts et al. (2016), and Colgan et al. (2018); uncertainties quoted are 2σ; *n*—number of samples. $^{206}Pb/^{238}U$ zircon ages were compiled from Watts et al. (2016), Colgan et al. (2018), and this study; uncertainties quoted are 95% confidence intervals; *n*—number of analyses. O isotope data were determined by laser fluorination for quartz and secondary ion mass spectrometry (SIMS) for zircon; uncertainties quoted are 1 standard deviation of combined analyses; *n*—number of analyses. VSMOW—Vienna standard mean ocean water.

*Multimodal $\delta^{18}O$ spectra; see Figure 5 and Supplementary Data Table DR2. Sr isotope data were compiled from John (1995), Varve (2013), Watts et al. (2016), and this study. John (1995) data were recalculated for the most up-to-date age data shown in the table; "–" indicates no data.

†Magma $\delta^{18}O$ values were calculated based on average $\Delta^{18}O_{quartz\text{-}melt}$ = 0.4‰ and $\Delta^{18}O_{melt\text{-}zircon}$ = 1.5‰ (fractionation factors from Trail et al. [2009] for 750–850°C: $\Delta^{18}O_{quartz\text{-}melt}$ = 0.4‰–0.5‰ and $\Delta^{18}O_{melt\text{-}zircon}$ = 1.4‰–1.7‰).

sections of five samples of the tuff of Elevenmile Canyon were analyzed with a JEOL 8900 electron microprobe at the USGS Menlo Park microanalytical facility. Mapping of individual hornblende crystals with a petrographic microscope and SEM enabled targeting of core and rim domains. The electron microprobe was operated at a 15 kV accelerating voltage, with a 10 nA defocused (5-µm-diameter) beam. A series of USGS mineral and major-oxide standards was used to monitor instrument drift and correct compositional offsets. Data for two additional samples of the tuff of Elevenmile Canyon, published in the M.S. thesis of Stepner (2017), are synthesized with our new data.

RESULTS

Oxygen and Strontium Isotope Data for Caldera-Forming Tuffs in the Western Nevada Volcanic Field in the Context of Regional Basement

Magmatic $\delta^{18}O$ values were calculated from quartz or zircon analyses for 16 caldera-forming tuffs in the western Nevada volcanic field. Units for which we have both quartz and zircon data indicate consistency in calculated magmatic (melt) values using fractionation factors from Trail et al. (2009) for $\delta^{18}O_{quartz\text{-}melt}$ = 0.4‰ and $\delta^{18}O_{melt\text{-}zircon}$ = 1.5‰ (Table 1). Calculated magmatic $\delta^{18}O$ values for the tuffs span from ~10‰ to 5.5‰ across a longitudinal profile from –116.8°W to –118.3°W (Figs. 1 and 3; Table 1). Whole-rock $^{87}Sr/^{86}Sr_i$ ratios for the same units were included for nine of these tuffs and span from ~0.707 to 0.705. These new data were plotted with available oxygen isotope data for regional granites (and strontium, where it exists for equivalent units) across the state of Nevada (Figs. 1 and 3; Supplementary Data Table DR1[1]). Most of these regional granites are Cretaceous or Jurassic in age, with magmatic $\delta^{18}O$ values calculated from quartz and zircon analyses (King et al., 2004), and fewer approximated from whole-rock $\delta^{18}O$ analyses (Wooden et al., 1999). Magmatic $\delta^{18}O$ values approximated from whole-rock analyses may be affected by alteration, whereas those calculated from zircon are free of these effects (e.g., Lackey et al., 2008).

A clearly defined gradient in both oxygen and strontium isotopes is apparent as the longitudinal profile steps west from the ~0.708 Sr_i isopleth, which marks the western boundary of the Precambrian craton in eastern Nevada, across a crustal transition zone, and into accreted arc terranes at the ~0.706 Sr_i isopleth (Fig. 3). The oxygen isotope gradient is broadly apparent in the regional Mesozoic granites, as first recognized by Solomon and Taylor (1989) and later refined by King et al. (2004), who concluded that granites east of the 0.706 Sr_i isopleth have a crustal signature indicative of high-$\delta^{18}O$ sedimentary components derived from the continental margin, with the edge at approximately the 0.708 Sr_i isopleth. For the middle Cenozoic calderas that are the focus of this investigation, the gradient closely mirrors that of the Mesozoic granitic basement, and it is bracketed by the high-$\delta^{18}O$ Caetano Tuff in central Nevada ($\delta^{18}O_{magma}$ = 10.2‰; $^{87}Sr/^{86}Sr_i$ = 0.7068–0.7072) and two low-$\delta^{18}O$ rhyolites of the Stillwater caldera complex in western Nevada, the tuffs of Poco Canyon and Job Canyon ($\delta^{18}O_{magma}$ = 5.5‰–6‰; $^{87}Sr/^{86}Sr_i$ = 0.7049–0.7057) (Figs. 1 and 3).

Nested calderas of the Stillwater complex have highly diverse magmatic $\delta^{18}O$ values; tuffs span from 5.5‰ to 8.7‰ (Fig. 3A; Table 1). In comparison, $^{87}Sr/^{86}Sr_i$ ratios for the same units appear to be less heterogeneous, spanning from 0.7049 to 0.7057 (Fig. 3B; Table 1). The Stillwater complex is the only documented locality with low-$\delta^{18}O$ magmas in the region. The Mount Jefferson caldera system, southeast of the Stillwater complex, also displays heterogeneity in successively erupted tuffs; the upper tuff of Mount Jefferson is ~1‰ lower that the lower tuff of Mount Jefferson (Fig. 3A; Table 1). Just south of the Mount Jefferson calderas, the Manhattan caldera may partly overlap the mineralized Round Mountain caldera, which hosts one of the largest epithermal gold deposits in the Great Basin (cf. Henry and John, 2013). The Manhattan caldera is distinctly lower in $\delta^{18}O$ compared to other calderas at this longitude in the O-Sr profile (Fig. 3A). In contrast, nested calderas of the central Nevada volcanic field studied by Larson and Taylor (1986) have consistently high and homogeneous $\delta^{18}O$ values (Fig. 3A), based on their analysis of bulk mineral separates. The high level of $\delta^{18}O$ diversity observed in nested calderas at Stillwater, Mount Jefferson, and potentially Manhattan, is not observed in different units within single (isolated) calderas in the western Nevada volcanic field, such as the Caetano caldera (Watts et al., 2016).

Three Cretaceous granitic plutons with outcrops around the Stillwater caldera complex, the Alameda Canyon to the north and the La Plata Canyon and Sand Springs to the south (Fig. 1), have high and variable magmatic $\delta^{18}O$ values: ~11‰ for Alameda Canyon, ~10‰ for La Plata Canyon, and ~8‰–9‰ for Sand Springs (Fig. 3A; Table 1). Only Sand Springs overlaps the upper range of Stillwater tuffs. Whole-rock $^{87}Sr/^{86}Sr_i$ ratios for Alameda Canyon (0.7050) and La Plata Canyon (0.7051) overlap Stillwater tuffs, whereas Sand Springs has distinctly lower $^{87}Sr/^{86}Sr_i$ (0.7043–0.7047) (Fig. 3B; Table 1). Therefore, none of these plutons is an isotopic match in oxygen and strontium for the Stillwater tuffs. However, other Cretaceous plutons in the vicinity do overlap the isotopic compositions of the Stillwater tuffs, such as the New York Canyon granite stock, ~40 km north in the Stillwater Range (Fig. 1), which has a whole-rock $\delta^{18}O$ value of 8.9‰ and $^{87}Sr/^{86}Sr_i$ ratio of 0.7056 (Figs. 3A–3B; Supplementary Data Table DR1), and the Rocky Canyon granitic pluton, ~80 km north intruding the Triassic Koipato Group in the West Humboldt Range (Fig. 1), which has a $^{87}Sr/^{86}Sr_i$ ratio of 0.7051 (Fig. 3B; Supplementary Data Table DR1). The Jurassic Humboldt mafic complex, which has extensive gabbroic and basaltic outcrops within ~20–40 km of the northern margin of the Stillwater caldera complex (Fig. 1), has unequivocally mantle-derived $^{87}Sr/^{86}Sr_i$ ratios (0.7041–0.7043) that are far lower than those found for any Stillwater units (Fig. 3B; Supplementary Data Table DR1).

Zircon U-Pb Ages and Inheritance in the Stillwater Caldera Complex in the Context of Regional Basement

Zircon $^{206}Pb/^{238}U$ ages have been determined by SHRIMP-RG for the 22 samples of the Stillwater caldera complex investigated for zircon O isotopes by SIMS (Table 2). As described by Colgan et al. (2018), U-Pb ages are bimodal, with the Job Canyon pulse at ca. 29 Ma and the Louderback Mountains, Poco Canyon, and Elevenmile Canyon pulses at ca. 25 Ma (Table 2). One sample from the Poco Canyon cycle and two from the Job Canyon cycle have inherited zircon grains, with U-Pb ages that are Eocene (35 Ma), Late Cretaceous (76–71 Ma, 98–95 Ma), Late Jurassic (150 Ma), Middle Jurassic (166 Ma), and Neoproterozoic (545 Ma) (Fig. 4A). Of the three Cretaceous granitic plutons analyzed, Alameda Canyon (84 Ma), La Plata Canyon (87 Ma), and Sand Springs (89 Ma), Alameda Canyon and La Plata Canyon have inherited grains that are Late Cretaceous (96 Ma), Early Cretaceous (104–102 Ma), and Triassic (203 Ma) (Fig. 4A). Two inherited Job Canyon zircons overlap Sand Springs zircons in both U-Pb age and $\delta^{18}O$ at ~6.6‰ (Fig. 4A, inset). In contrast, one Job Canyon grain is much older at 150 Ma, though overlapping in

[1]GSA Data Repository item 2019060, O and Sr isotope and age data for regional basement rocks in the Great Basin, zircon O isotope, age and trace element data for the Stillwater caldera complex, and hornblende chemistry data for the tuff of Elevenmile Canyon, is available at http://www.geosociety.org/datarepository/2019 or by request to editing@geosociety.org.

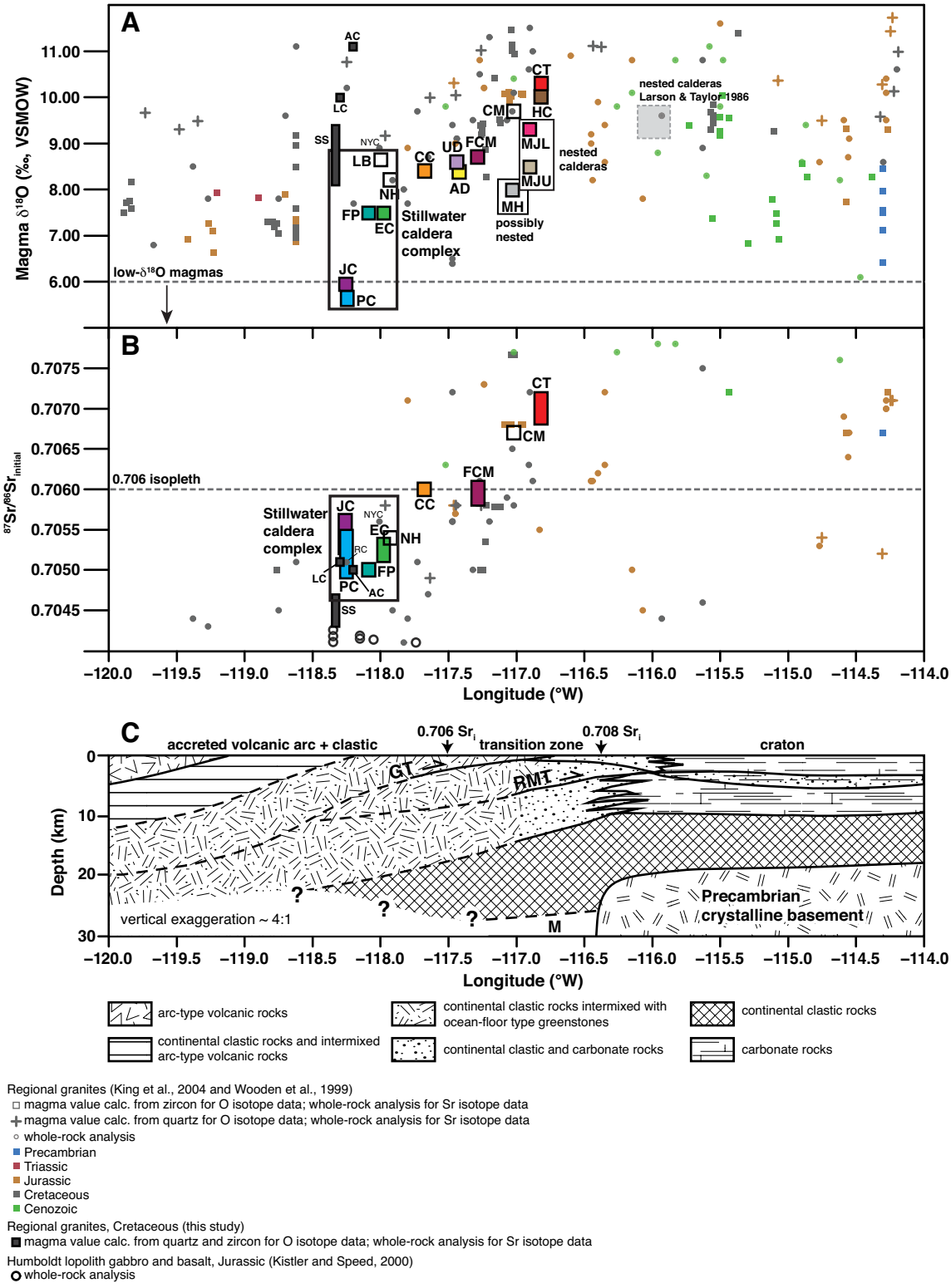

Figure 3. Longitudinal profiles for (A) magmatic $\delta^{18}O$ and (B) $^{87}Sr/^{86}Sr_i$ values for calderas of the western Nevada volcanic field, with labels that correspond to those in Figure 1 and data in Table 1. Unfilled boxes indicate uncertain caldera locations. Included in these plots are published $\delta^{18}O$ data for regional granites, and, when available for the same units, $^{87}Sr/^{86}Sr_i$ (see Supplementary Data Table DR1 for compilation of all plotted data). The low-$\delta^{18}O$ magma threshold ($\delta^{18}O$ = 6‰) is based on closed-system differentiation of mantle basalt (Bindeman, 2008). (C) Generalized pre-Jurassic crustal profile at ~40°N latitude in central Nevada, shown for the same longitudinal scale, adapted after Farmer and DePaolo (1983) and King et al. (2004). Depths are pre-Jurassic; they do not account for Jurassic–Cretaceous crustal shortening or Cenozoic extension. GT—Golconda thrust, RMT—Roberts Mountains thrust, M—mantle.

TABLE 2. SUMMARY OF OXGYEN ISOTOPE DATA FOR THE STILLWATER CALDERA COMPLEX

Caldera cycle	Unit	Sample(s)	Age (Ma)	SIMS data, $\delta^{18}O$ (‰, VSMOW)		Laser fluorination data, $\delta^{18}O$ (‰, VSMOW)						
				Zircon range*	Zircon average†	Zircon	Quartz	Sanidine	Plagioclase	Biotite	Magma§	$\Delta^{18}O_{quartz\text{-}zircon}$ T# (°C)
Job Canyon	Pre–Job andesite/dacite	13-DJ-11	29.38 ± 0.38	7.0–8.6 (17/17)	7.21 ± 0.11 (12/17)	–	–	–	–	–	8.71	–
Job Canyon	Pre–Job dacite tuff	10-DJ-5	29.32 ± 0.97	6.5–7.7 (25/26)	6.98 ± 0.24 (25/25)	–	–	–	–	–	8.48	–
Job Canyon	Tuff of Job Canyon	10-DJ-2	29.25 ± 0.47	4.2–6.8 (20/20)	4.49 ± 0.26 (19/20)	4.10, 4.69	–	–	–	–	5.99	–
Job Canyon	Post–Job andesite/dacite	10-DJ-3; 13-DJ-46 (LF)	28.54 ± 0.51	4.0–8.1 (20/24)	5.41 ± 0.25 (10/20)	–	–	–	6.55, 6.56	5.33, 5.42	6.91	–
Job Canyon	IXL pluton	JC08-IXL4	28.45 ± 0.35	5.8–6.8 (14/14)	6.24 ± 0.27 (14/14)	6.00	8.68, 8.51	–	–	–	7.74	721, 787
Job Canyon	IXL pluton	JC08-IXL2	28.07 ± 0.33	6.2–6.6 (15/15)	6.34 ± 0.11 (15/15)	6.27	–	–	–	–	7.84	–
Louderback Mountains	Louderback Mountains rhyolite	12-DJ-34	25.52 ± 0.25	4.5–7.4 (14/14)	7.24 ± 0.11 (12/14)	–	–	–	–	–	8.74	–
Louderback Mountains	Tuff of Louderback Mountains	13-DJ-7	25.29 ± 0.26	3.9–7.3 (14/14)	7.09 ± 0.23 (5/14)	–	–	–	–	–	8.59	–
Louderback Mountains	Chalk Mountain pluton	JC11-26	25.05 ± 0.26	4.9–6.1 (15/15)	5.77 ± 0.17 (14/15)	–	–	–	–	–	7.27	–
Louderback Mountains	Chalk Mountain porphyry	JC11-32	25.04 ± 0.32	5.4–6.2 (14/14)	5.73 ± 0.25 (14/14)	–	–	–	–	–	7.23	–
Poco Canyon	Breccia-rich tuff of Poco Canyon	10-DJ-6	25.99 ± 0.20	3.9–4.7 (20/20)	4.25 ± 0.21 (20/20)	–	–	–	–	–	5.75	–
Poco Canyon	Lower tuff of Poco Canyon	12-DJ-38	25.74 ± 0.19	3.6–6.9 (29/30)	4.03 ± 0.21 (25/29)	4.07	6.16, 6.28	–	–	–	5.53	757, 825
Poco Canyon	Tuff of Poco Canyon	10-DJ-4	25.60 ± 0.25	4.0–6.3 (22/22)	4.32 ± 0.15 (14/22)	4.92, 5.25	6.66, 6.88	6.35	–	–	5.82	702, 765
Poco Canyon	Rhyolite of Coyote Canyon	JC13-9	25.24 ± 0.25	4.0–4.7 (15/15)	4.27 ± 0.17 (15/15)	–	–	–	–	–	5.77	–
Poco Canyon	Freeman Creek pluton, granite	JC08-IXL8	24.93 ± 0.37	5.5–6.4 (17/17)	5.66 ± 0.14 (15/17)	4.74, 5.47	–	–	–	–	7.16	–
Elevenmile Canyon	Tuff of Lee Canyon	12-DJ-36	25.57 ± 0.26	4.2–7.1 (20/20)	6.03 ± 0.29 (16/20)	6.13	7.88, 8.21	6.81	–	–	7.53	804, 872
Elevenmile Canyon	Tuff of Hercules Canyon	12-DJ-33	25.37 ± 0.19	5.4–7.4 (20/20)	6.02 ± 0.28 (16/20)	5.78, 5.87	7.68, 7.91	–	7.40, 7.50	–	7.52	873, 945
Elevenmile Canyon	Tuff of Elevenmile Canyon	H00-104A	25.23 ± 0.26	4.9–7.9 (19/19)	6.03 ± 0.51 (13/19)	5.70, 5.71	7.38, 8.06, 8.35	7.05	–	–	7.53	834, 903
Elevenmile Canyon	Tuff of Elevenmile Canyon	14-DJ-79	25.20 ± 0.30	4.2–6.5 (14/14)	5.95 ± 0.31 (12/14)	–	8.32, 8.46	–	–	–	7.45	704, 767
Elevenmile Canyon	Freeman Creek pluton, granodiorite	12-DJ-35	25.16 ± 0.23	5.2–7.7 (19/19)	5.80 ± 0.33 (11/19)	5.37, 5.66	–	–	–	–	7.30	–
Elevenmile Canyon	Tuff of Elevenmile Canyon	12-DJ-37	25.12 ± 0.31	5.9–8.2 (16/16)	6.11 ± 0.13 (8/16)	–	–	–	–	–	7.61	–
Elevenmile Canyon	Tuff of Elevenmile Canyon	14-DJ-75A	25.00 ± 0.26	3.9–7.1 (23/23)	5.86 ± 0.15 (8/23)	6.02, 6.20	8.28	–	–	–	7.36	708, 772

Note: Ages are error-weighted mean zircon $^{206}Pb/^{238}U$ ages; data are from Colgan et al. (2018); "–" indicates no data. SIMS—secondary ion mass spectrometry; VSMOW—Vienna standard mean ocean water.

*Numbers in parentheses are number of analyses out of total number of analyses used to define range (Mesozoic and Cenozoic xenocrysts excluded); see Supplementary Data Table DR2 for full data set.

†Dominant (and/or rim) peak in spectra was used to calculate average; uncertainties quoted are 1 standard deviations of combined analyses; *n*—number of analyses out of defined range used to calculate average; see Supplementary Data Table DR2 for full data set.

§Magma $\delta^{18}O$ values were calculated based on average $\Delta^{18}O_{quartz\text{-}melt}$ = 0.4‰ and $\Delta^{18}O_{melt\text{-}zircon}$ = 1.5‰ (fractionation factors from Trail et al. [2009] for 750–850 °C; $\Delta^{18}O_{quartz\text{-}melt}$ = 0.4‰–0.5‰ and $\Delta^{18}O_{melt\text{-}zircon}$ = 1.4‰–1.7‰). The calibration of Lackey et al. (2008) for whole-rock wt% SiO_2 (~65–78 wt%) results in calculated magma $\delta^{18}O$ values that are ~0‰–0.5‰ higher.

#Equilibrium $\Delta^{18}O_{quartz\text{-}zircon}$ temperatures were calculated with fractionation factors from Trail et al. (2009) and Valley et al. (2003); the latter reference yields ~60–70 °C higher temperatures.

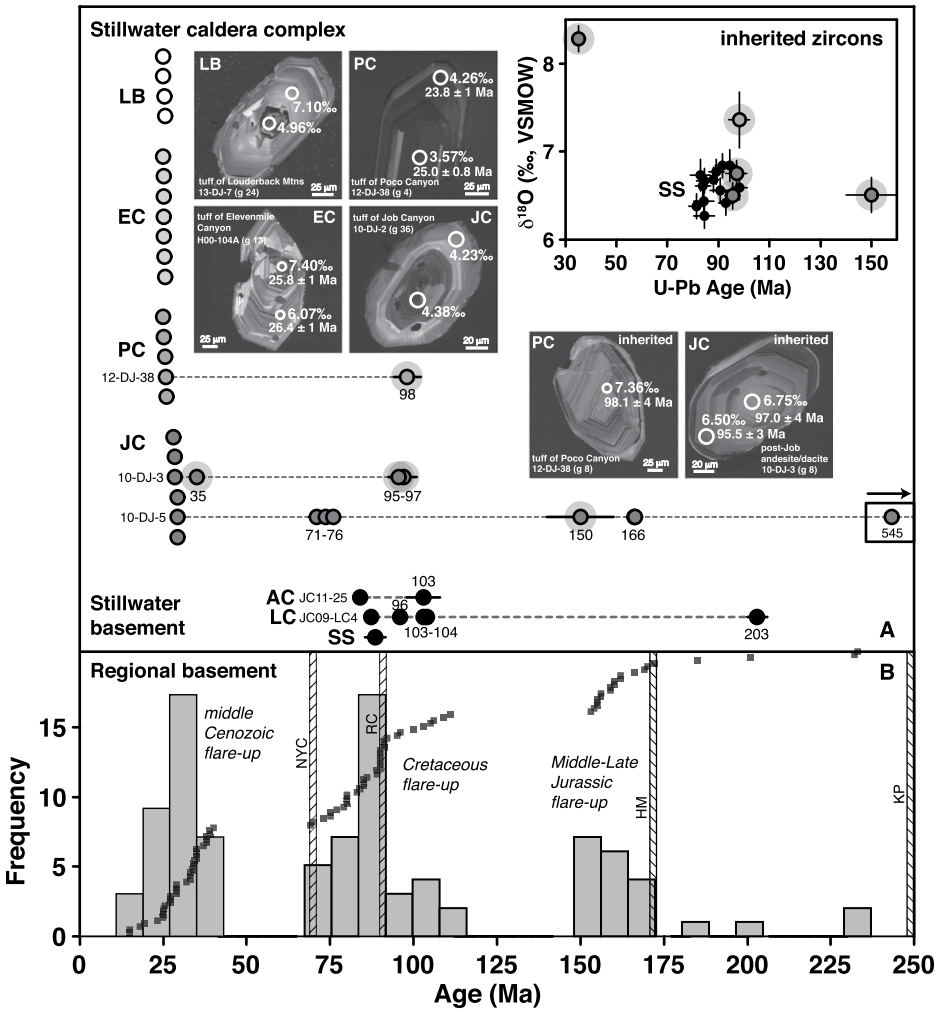

Figure 4. Zircon $^{206}Pb/^{238}U$ ages and inheritance in units of the Stillwater caldera complex in the context of regional basement. Labels correspond to those in Figure 1. (A) Weighted mean zircon $^{206}Pb/^{238}U$ ages for studied samples of the Stillwater caldera complex and Stillwater basement plutons are shown by the circle symbols (data listed in Tables 1 and 2), and samples with inheritance are shown by the dashed lines that extend to the inherited grains with their ages labeled. Zircon cathodoluminescence (CL) images are shown for selected samples with analytical spots labeled for $\delta^{18}O$ values and $^{206}Pb/^{238}U$ ages. Inset in A shows $\delta^{18}O$ values and $^{206}Pb/^{238}U$ ages for inherited zircons in the Stillwater caldera complex compared to zircons in the Cretaceous Sand Springs pluton; highlighted gray circles show the grains in the main panel. (B) Histogram of Cenozoic and Mesozoic age data for regional basement units in the Great Basin, Nevada (individual units are shown by gray squares overlying the histogram; data are tabulated in Supplementary Data Table DR1). Ages were excluded if they did not overlap within 5% error for the same units in King et al. (2004) and Wooden et al. (1999). If the ages overlapped, but were not identical, an intermediate age was used. Each unit is only represented once. The striped vertical bars in B show the ages of specific basement units that may be pertinent to understanding the Stillwater basement architecture, including the New York Canyon (NYC) stock, the Rocky Canyon (RC) pluton, Humboldt mafic complex (HM), and the Koipato (KP) Group volcanics.

$\delta^{18}O$, and another is much younger at 35 Ma and distinctly higher in $\delta^{18}O$ at ~8.3‰ (Fig. 4A, inset). One inherited Poco Canyon zircon overlaps Sand Springs in U-Pb age but is slightly higher in $\delta^{18}O$ at ~7.4‰ (Fig. 4A, inset).

Age data for regional basement rocks and Cenozoic calderas define three major pulses, or flare-ups, of silicic igneous activity in the middle Cenozoic, Cretaceous, and Middle–Late Jurassic (Fig. 4B). Inherited zircons in the Stillwater caldera complex and Stillwater basement plutons fall broadly into these flare-up time periods, and most inherited zircons are Cretaceous in age (Figs. 4A–4B). Ages of specific basement units discussed in the previous section on oxygen and strontium isotopes are as follows: New York Canyon granite stock (ca. 71–69 Ma), Rocky Canyon granitic pluton (ca. 92–90 Ma), Humboldt mafic complex (ca. 172–169 Ma), and Koipato Group volcanics (ca. 250–248 Ma) (Fig. 4B; age data from Johnson, 1977; Wooden et al., 1999; Kistler and Speed, 2000; Vikre, 2014). Of these, all but the Koipato Group have ages that overlap within error with the inherited zircon ages documented in the Stillwater caldera complex (Figs. 4A–4B).

Oxygen Isotope Evolution in the Stillwater Caldera Complex

Oxygen isotope ratios collected by SIMS for 22 samples and ~400 analytical spots for single zircons are synthesized in Figure 5 and Table 2 (full data in Supplementary Data Table DR2). Laser fluorination data for bulk zircon and major phenocryst phases of quartz, sanidine, plagioclase, and biotite are included for 13 samples (Fig. 5; Table 2).

Job Canyon cycle magmatism began with andesite and dacite lava flows and small explosive eruptions (Fig. 5A). These units have high-$\delta^{18}O_{zircon}$ values of 7.0‰–7.2‰ and $\delta^{18}O_{magma}$ of 8.5‰–8.7‰. The caldera-forming eruption of the tuff of Job Canyon was the first low-$\delta^{18}O$ rhyolite produced, with $\delta^{18}O_{zircon}$ of 4.5‰ and $\delta^{18}O_{magma}$ of 6.0‰. Bulk zircon analyzed by laser fluorination is in agreement with the SIMS zircon data ($\delta^{18}O_{zircon}$ = 4.1‰–4.7‰). Next erupted was one of the most heterogeneous units documented in the Stillwater caldera complex, the post–Job Canyon andesite/dacite lava, with $\delta^{18}O_{zircon}$ that spans from 4.0‰ to 8.1‰. Plagioclase and biotite analyzed by laser fluorination are in high-temperature equilibrium (i.e., >700 °C) with the magmatic $\delta^{18}O$ composition calculated from zircon rims. In addition to having the largest overall $\delta^{18}O$ range in zircons, the post–Job Canyon andesite/dacite also has the largest $\delta^{18}O$ variation within single zircons (>2‰ zoning between core, interior,

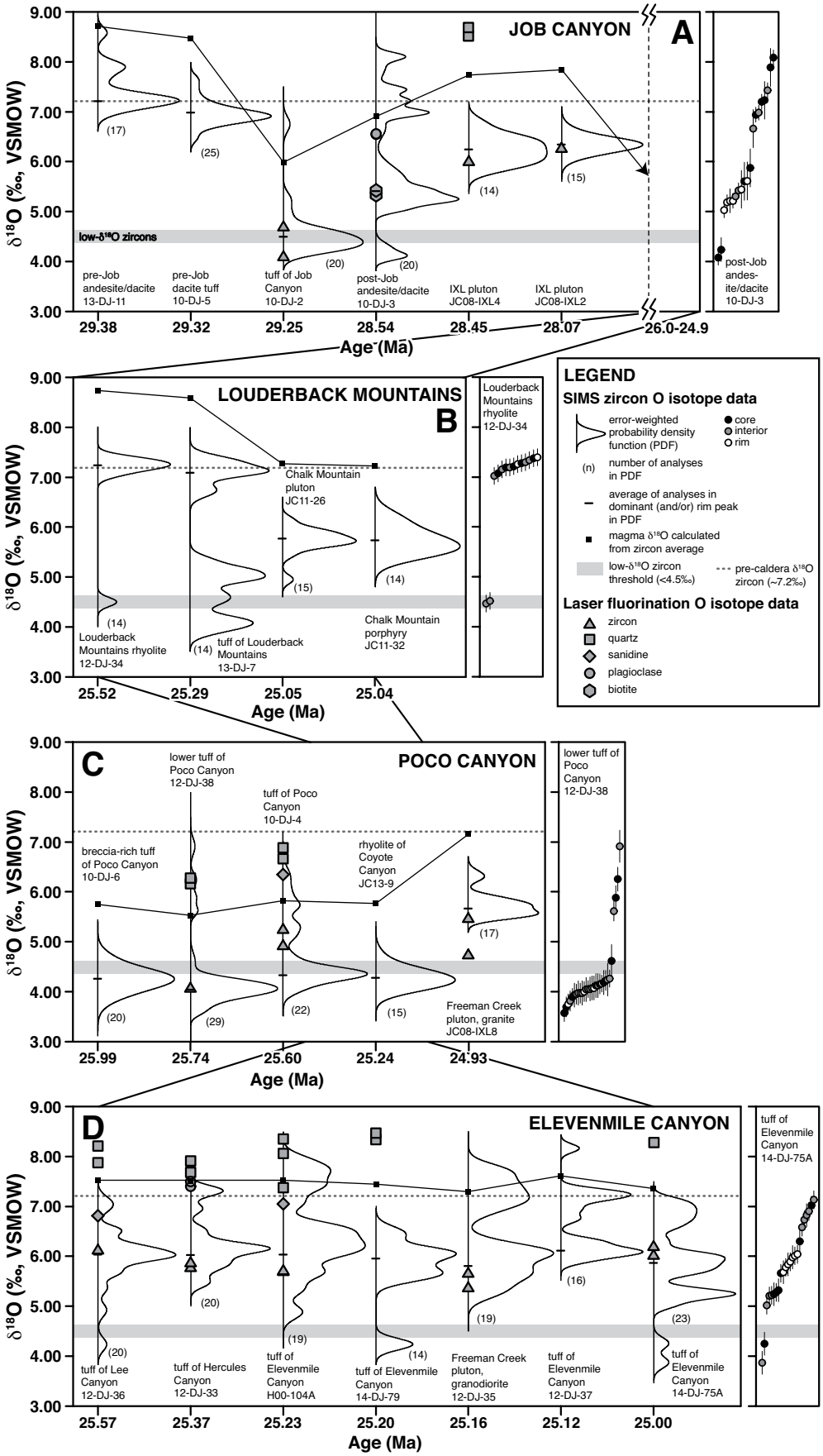

Figure 5. Oxygen isotope evolution of the Stillwater caldera complex, with units of each caldera cycle plotted in order of their error-weighted mean $^{206}Pb/^{238}U$ zircon ages; tie lines between panels show age overlaps. Secondary ion mass spectrometry (SIMS) zircon oxygen isotope data are shown by error-weighed probability density functions (PDFs), constructed using Isoplot (Ludwig, 2012). On the right side of each panel are rank-order plots that show the individual zircon data used to construct PDFs for an example sample. Data are summarized in Table 2 and included in full in Supplementary Data Table DR2. Laser fluorination oxygen isotope data for bulk zircon and other mineral phases are shown by the symbols plotted over the PDFs. The calculated magmatic $\delta^{18}O$ values for each sample are connected by thin black lines. The pre-caldera (i.e. pre–Job andesite/dacite) $\delta^{18}O$ zircon boundary (~7.2‰) is shown by the horizontal gray dashed line, and the threshold for low-$\delta^{18}O$ zircons (<4.5‰) is shown by the horizontal gray bar.

and rim domains). Intrusion of the IXL pluton marked a return to normal-$\delta^{18}O$ values in the Job Canyon cycle, with $\delta^{18}O_{zircon}$ of 6.2‰–6.3‰ and $\delta^{18}O_{magma}$ of 7.7‰–7.8‰. The IXL pluton samples are the most homogeneous of all Job Canyon cycle units, with unimodal probability density functions (PDFs) and zircons that are unzoned or very subtly zoned in $\delta^{18}O$. Laser fluorination data for bulk zircon from the IXL pluton are identical within error to the SIMS data, and laser fluorination data for quartz are in high-temperature equilibrium with zircon.

The next major caldera cycle in the Stillwater complex resumed after a long hiatus (>2 m.y.) with the eruption of the tuff of Louderback Mountains (Fig. 5B). The tuff of Louderback Mountains has a multimodal PDF, with both low-$\delta^{18}O$ and high-$\delta^{18}O$ zircons, and it is distinctly lacking in zircons with $\delta^{18}O$ of ~6‰, which defined zircons at the end of the Job Canyon cycle. The Louderback Mountains rhyolite, a lava or intrusion underlying the tuff of Louderback Mountains, has zircons with a very similar distribution to the tuff of Louderback Mountains; zircon rims in this sample are 7.2‰–7.4‰. The dominant PDF peak and rim analyses in the Louderback Mountains rhyolite correspond to $\delta^{18}O_{zircon}$ of 7.1‰–7.2‰ and $\delta^{18}O_{magma}$ of 8.6‰–8.7‰. Two intrusive units that underlie the Louderback Mountains caldera, the Chalk Mountain pluton and porphyry, have zircon populations that are very similar to one another, but very different from the tuff of Louderback Mountains. The Chalk Mountain units are unimodal, with the exception of one zircon with slightly lower $\delta^{18}O$ in the pluton. The dominant peak and rim analyses correspond to $\delta^{18}O_{zircon}$ of 5.7‰–5.8‰ and $\delta^{18}O_{magma}$ of 7.2‰–7.3‰.

The Poco Canyon caldera cycle succeeded the Louderback Mountains caldera cycle (Fig. 5C). All samples of the tuff of Poco Canyon are low-$\delta^{18}O$ rhyolites, with $\delta^{18}O_{zircon}$ of 4.0‰–4.3‰ and $\delta^{18}O_{magma}$ of 5.5‰–5.8‰. Two samples of the tuff (lower and upper cooling units) have multimodal PDFs with a small proportion (~15%–35%) of normal-$\delta^{18}O$ zircons. Laser fluorination data for quartz and sanidine are in high-temperature equilibrium with the dominant PDF peaks for Poco Canyon zircons. The rhyolite of Coyote Canyon, which is a lava that preceded the tuff, has a unimodal zircon PDF that is identical to the dominant PDF peaks in the tuff of Poco Canyon. The granitic phase of the Freeman Creek pluton, which underlies the Poco Canyon caldera, has zircons that are significantly higher in $\delta^{18}O$, with $\delta^{18}O_{zircon}$ of 5.7‰ and $\delta^{18}O_{magma}$ of 7.2‰. Laser fluorination data for bulk zircon overlap the SIMS zircon data for one analysis, but a duplicate analysis was ~0.9‰ lower. This fact, combined with the bimodal PDF for the granitic phase of the Freeman Creek pluton, indicates that it may be more heterogeneous than the current data show.

The Elevenmile Canyon caldera cycle is the youngest and most voluminous of the Stillwater caldera complex and overlapped the Poco Canyon cycle in space and time; however, the Elevenmile Canyon cycle has an oxygen isotope record that is highly disparate from the Poco Canyon cycle (Fig. 5D). All samples of the tuff of Elevenmile Canyon (and equivalent tuffs of Lee and Hercules Canyon from previous nomenclature of John [1995] and Henry and John [2013]) have multimodal PDFs with $\delta^{18}O_{zircon}$ that spans from 4.2‰ to 8.2‰. Low-$\delta^{18}O$ zircons were found in three of the six tuff samples studied. The dominant PDF peaks have $\delta^{18}O_{zircon}$ of 5.9‰–6.1‰ ($\delta^{18}O_{magma}$ of 7.4‰–7.6‰), which is consistent with the laser fluorination data for bulk zircon, and in high-temperature equilibrium with the laser fluorination data for

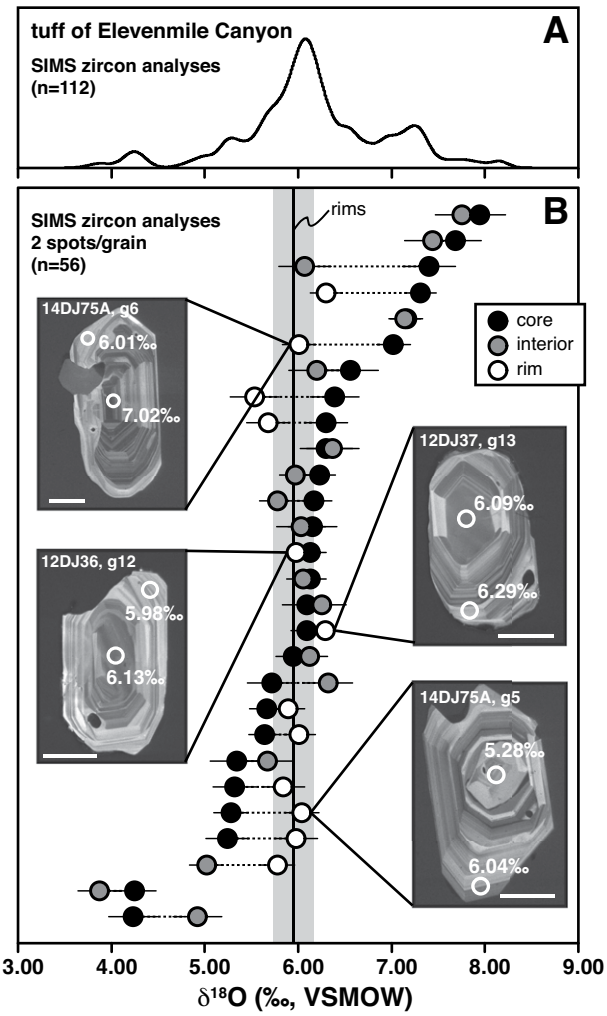

Figure 6. Oxygen isotope data for zircons of the tuff of Elevenmile Canyon determined by ion microprobe: (A) error-weighted probability density function for all zircon analyses, and (B) rank-order plot for zircons with two analytical spots per grain. Horizontal dashed lines connect core, interior, and/or rim analyses for individual grains. Vertical black line shows the average and standard deviation of only rim analyses. Zircon cathodoluminescence (CL) images annotated with $\delta^{18}O$ values for core and rim analyses are shown for a few representative grains. White bar at the bottom of each CL image is 50 µm.

quartz, sanidine, and plagioclase. Single zircons in the tuff of Elevenmile Canyon are commonly zoned, with lower- and higher-$\delta^{18}O$ cores and interiors overgrown by homogeneous rims with an average $\delta^{18}O$ of 5.9‰ ± 0.2‰ (n = 12 rims; 1 standard deviation), which approximates the dominant PDF peak for all tuff of Elevenmile Canyon zircon analyses combined (n = 112; Fig. 6). The granodiorite phase of the Freeman Creek pluton has a multimodal zircon PDF that is very similar to the tuff of Elevenmile Canyon, with $\delta^{18}O_{zircon}$ of 5.8‰ for the dominant peak. Laser fluorination data for bulk zircon in the Freeman Creek pluton granodiorite are consistent with the SIMS data.

Trace elements were collected for a subset of the zircons analyzed for oxygen isotopes from the Job Canyon, Poco Canyon, and Elevenmile Canyon caldera cycles (Fig. 7; Supplementary Data Table DR2). Hafnium contents of zircons vary from ~5000 to 12,000 ppm for high-, normal-, and low-$\delta^{18}O$ zircons (Figs. 7A, 7C, and 7E). Low-$\delta^{18}O$ zircons in the Job Canyon cycle have relatively restricted Hf (~6000–7000 ppm), while those in the Poco Canyon cycle span almost the full range of Hf represented in the Stillwater caldera complex (~6000–12,000 ppm). Low-$\delta^{18}O$ zircons in the Elevenmile Canyon cycle are few in comparison; the two for which we have Hf data are ~9000 ppm. Each cycle

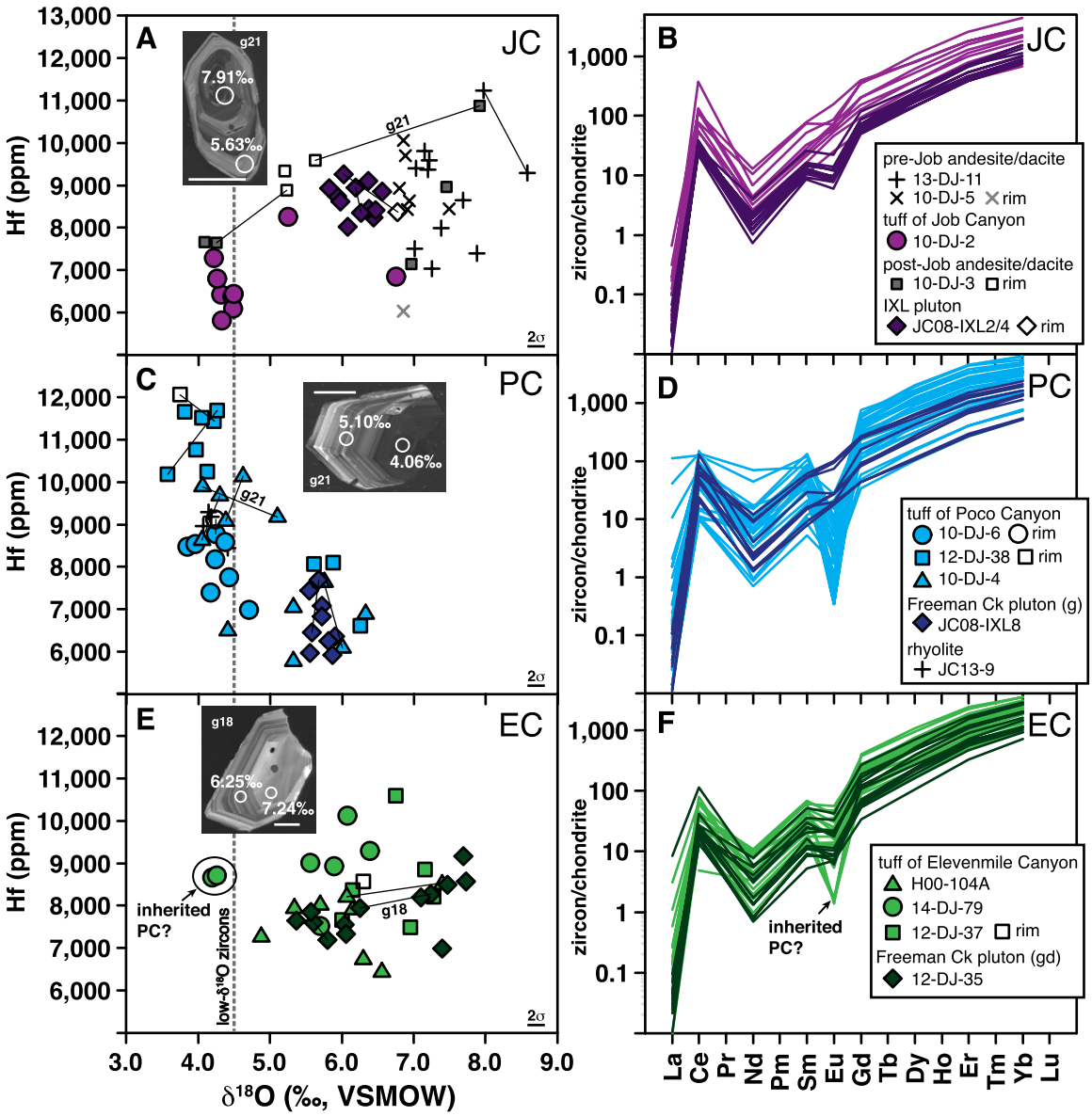

Figure 7. Hafnium, $\delta^{18}O$, and rare earth element (REE) data for single zircons in the Stillwater caldera complex determined by ion microprobe (Supplementary Data Table DR2). Labels correspond to those in Figure 1. Vertical dashed gray line in the left panels shows the threshold for low-$\delta^{18}O$ zircons (<4.5‰). Tie lines connect analytical spots within the same grains, with grain numbers labeled for those with a corresponding cathodoluminescence (CL) image in the left panels. White bar at the bottom of each CL image is 50 µm; g—granite, gd—granodiorite. In panels E and F, grains interpreted to be inherited from the Poco Canyon (PC) cycle are indicated.

possesses zircons with significant zoning in both $\delta^{18}O$ and Hf. The greatest zoning is observed in the post–Job Canyon andesite/dacite, which has highly heterogeneous core and interior zircon domains that are overgrown by homogenized rims with $\delta^{18}O$ of ~5.4‰ and Hf of ~9000 ppm (Fig. 7A). Chondrite-normalized rare earth element (REE) patterns in zircons from tuffs and plutons in the three cycles (Figs. 7B, 7D, and 7F), combined with the Hf and $\delta^{18}O$ data, indicate that zircons in the Job Canyon and Poco Canyon cycles have tuffs and plutons with distinctly different geochemical signatures (i.e., higher $\delta^{18}O$, higher Hf, and lower REEs in the IXL pluton compared to the tuff of Job Canyon, and higher $\delta^{18}O$, lower Hf, and higher REEs in the Freeman Creek pluton granite compared to the tuff of Poco Canyon). In contrast, zircons in the tuff of Elevenmile Canyon and Freeman Creek pluton granodiorite overlap in $\delta^{18}O$, Hf, and REEs. One of the most distinctive features of low-$\delta^{18}O$ zircons in the tuff of Poco Canyon is a sharp negative Eu anomaly (Fig. 7D). We note that zircons in the tuff of Louderback Mountains have REE and Hf contents similar to the Poco Canyon zircons (Colgan et al., 2018). Two low-$\delta^{18}O$ zircons in the tuff of Elevenmile Canyon share this geochemical characteristic (as well as $\delta^{18}O$ and Hf values that are within the range of Poco Canyon and Louderback Mountains zircons), suggesting that they are inherited from one of these cycles.

Hornblende Barometry Constraints for the Tuff of Elevenmile Canyon Magma Chamber

Hornblende chemistry was determined by electron microprobe for the tuff of Elevenmile Canyon to constrain crystallization pressures and estimate the crustal depths at which silicic magma chambers resided in the Stillwater caldera complex (Fig. 8; Supplementary Data Table DR3). The samples span ~20 km across the Louderback, Clan Alpine, and Desatoya Mountains and represent the trachydacitic-rhyolitic compositional range of the tuff (~62–73 wt% SiO_2). There are two distinct compositional groups of hornblende, a low-Al group with ~6–7.5 wt% Al_2O_3 and a high-Al group with ~10.5–12 wt% Al_2O_3 (Fig. 8A). The high-Al group has higher Mg, Ca, Ti, Na, and K and lower Si, Fe, and Cl relative to the low-Al group. Two samples have hornblende crystals that fall within each group, but the two groups do not overlap, and the high-Al hornblendes were only documented in samples with whole-rock SiO_2 less than 68 wt%. Single hornblende crystals are unzoned or very subtly zoned from core to rim (e.g., Figs. 8B–8C).

Two Al-in-amphibole geobarometers (Ridolfi et al., 2010; Mutch et al., 2016) were used to estimate crystallization pressures for the two hornblende groups. The results between the two geobarometers are disparate for the same hornblende Al contents (vary by about a factor of two), and because it is not clear which geobarometer may be more accurate (and because Al-in-amphibole geobarometry is prone to large uncertainties in general; Putirka, 2016), we make very general estimates for crystallization pressures and depths for average compositions for the two hornblende groups. We note that the Mutch et al. (2016) barometer was calibrated for low-pressure granitic rocks with the same mineral assemblage that is found in Stillwater rhyolites. For the low-Al group, the intermediate total Al content (1.2 atoms per formula unit, apfu) corresponds to 1.0–2.2 kbar and ~4–8 km depth (based on a 3.7 km/kbar pressure-depth conversion) (Fig. 8A). For the high-Al group,

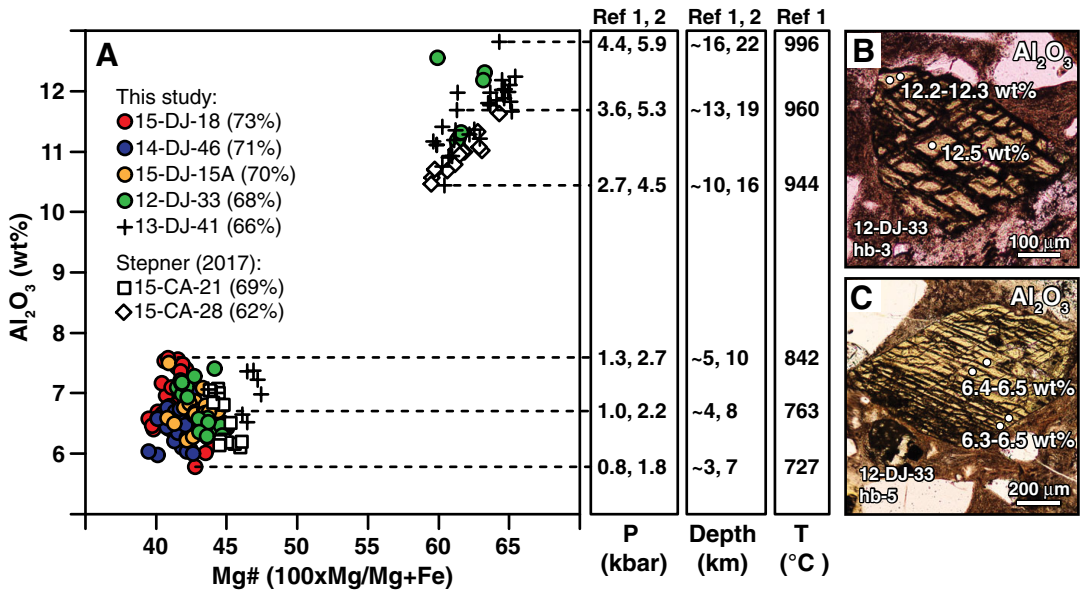

Figure 8. Hornblende geochemical data for the tuff of Elevenmile Canyon determined by electron microbe (Supplementary Data Table DR3). (A) Aluminum content vs. Mg#. Whole-rock SiO_2 contents of host tuff samples are shown in parentheses. Pressures (P) calculated with the barometers of Ridolfi et al. (2010) ("Ref 1") and Mutch et al. (2016) ("Ref 2") are connected by horizontal dashed lines to single hornblende analyses that span the compositional ranges of the two hornblende groups. Depths were estimated from calculated pressures with a 3.7 km/kbar conversion. Crystallization temperatures (T) of hornblende from the Ridolfi et al. (2010) calibration are included to the right. (B–C) Representative photomicrographs of high- and low-Al hornblende crystals in one of the tuff samples, showing a lack of zoning between core and rim domains.

the intermediate total Al content (2.0 apfu) corresponds to 3.6–5.3 kbar and ~13–19 km depth (Fig. 8A). Because the majority (~80%) of hornblende crystals fall within the low-Al group and do not define a continuum with the high-Al group, we interpret the ~4–8 km depth estimate as representative of the tuff of Elevenmile Canyon magma chamber, and the high-Al hornblendes as xenocrysts.

DISCUSSION

We begin the discussion by describing regional isotopic trends in Cenozoic and Mesozoic silicic magmas in the Great Basin, which we use to frame our study of the Stillwater caldera complex, one of the largest nested caldera centers of the middle Cenozoic ignimbrite flare-up. We consider potential crustal sources in the petrogenesis of isotopically diverse Stillwater magmas, beginning with the first Job Canyon caldera cycle and then subsequent caldera cycles, followed by an evaluation of possible low-$\delta^{18}O$ rhyolite genesis models. We conclude the discussion by assessing relationships between caldera-forming tuffs and plutons in the Stillwater caldera complex.

Significance of Regional Oxygen and Strontium Isotopic Trends in the Great Basin

The isotopic trends defined by our new data for voluminous caldera-forming tuffs of the western Nevada volcanic field reflect the basement crustal architecture, with the highest $\delta^{18}O$ values and $^{87}Sr/^{86}Sr_i$ ratios just west of the North American craton boundary at the 0.708 Sr_i isopleth, where the thickest packages of continental clastic rocks accumulated in the miogeocline (Figs. 1 and 3). The contribution of the clastic (meta)sediment package to silicic magmas appears to wane (lower $\delta^{18}O$, $^{87}Sr/^{86}Sr_i$) westward across the transition zone and into accreted oceanic terranes at the 0.706 Sr_i isopleth. The same trends in oxygen and strontium isotopes are broadly apparent in Jurassic and Cretaceous granites (Fig. 3), indicating that these trends are pre-Jurassic features; they reflect the Precambrian craton margin, passive-margin sedimentation, and Paleozoic tectonic events (Antler and Sonoma orogenies) that thickened the miogeoclinal sediment prism (Dickinson, 2006). The tighter trends resolved in the Cenozoic calderas may be a function of averaging of isotopic heterogeneities in the crustal block over tens of millions of years of silicic magmatism during the Jurassic and Cretaceous, with the Cenozoic calderas representing discrete point sources through the homogenized crustal block.

In addition to a trend of increasing sedimentary components in magmas from west to east, King et al. (2004) proposed an increase in the availability of sedimentary components through time as successive orogenic events thickened the crust, with Late Cretaceous granites having higher $\delta^{18}O$ values and $^{87}Sr/^{86}Sr_i$ ratios (and thus a greater crustal affinity) than Early Cretaceous and Jurassic granites, similar to the conclusions of Barton (1990). Our data demonstrate that middle Cenozoic calderas just west of the 0.708 Sr_i isopleth have highly elevated $\delta^{18}O$ values (e.g., $\delta^{18}O_{zircon}$ of 8.7‰ and $\delta^{18}O_{magma}$ of 10.2‰ for the Caetano Tuff) that are similar to values of Late Cretaceous granites emplaced during the Sevier orogeny at this longitude (cf. King et al., 2004). This indicates that orogenic events that thickened the crust in the Cretaceous continued to exert a control on the isotopic signatures of Cenozoic silicic magmas. Metapelite xenoliths, zircon inheritance, and Sr-Nd-O isotopic modeling support derivation of the Caetano Tuff from anatexis of Proterozoic metasedimentary basement crust (Watts et al., 2016). In contrast to the interpretation by King et al. (2004), for a greater mantle component in Cenozoic magmas due to crustal thinning during Basin and Range extension, it is now recognized that episodes of extension significantly postdated middle Cenozoic caldera magmatism (e.g., Colgan et al., 2008), and our oxygen and strontium isotope data do not support a greater mantle component in their source magmas as compared to Mesozoic granites at the same longitude (Fig. 3).

Several Cretaceous granitic plutons west of the 0.706 Sr_i isopleth that were analyzed in this study (Alameda Canyon, La Plata Canyon, Sand Springs) have much higher $\delta^{18}O$ values ($\delta^{18}O_{quartz}$ of 9.8‰–11.5‰ and $\delta^{18}O_{magma}$ of 8.1‰–11.1‰) than the O-Sr trends would predict for this location on the longitudinal profile (Fig. 3A). King et al. (2004) also documented several Cretaceous granites with high-$\delta^{18}O$ quartz values at approximately this longitude, which they attributed to subsolidus alteration of quartz rather than reflecting the isotopic composition of the host magmas. Our data indicate that these elevated $\delta^{18}O$ values may be primary (or close to primary), based on (1) the consistency of triplicate analyses for quartz in each of the three plutons, and (2) the high-temperature equilibrium of quartz with zircon for the Sand Springs pluton ($\delta^{18}O_{quartz\text{-}zircon}$ = 3.2‰, which corresponds to 580 °C or 635 °C equilibrium based on the fractionation factors of Trail et al. [2009] or Valley et al. [2003], respectively). The location of the plutons is coincident with back-arc basinal sedimentary terranes that were thrust onto the continental shelf during the Jurassic Luning-Fencemaker fold-and-thrust events (Wyld et al., 2003), indicating that their genesis may have involved contamination by these sedimentary sources. Though the $\delta^{18}O$ compositions of the plutons are elevated, their $^{87}Sr/^{86}Sr_i$ ratios (0.7043–0.7051) are consistent with the radiogenic signatures of other granites and caldera-forming tuffs at this longitude (Fig. 3B).

In broader applicability, the O-Sr longitudinal trends documented here, which represent isotopic sampling of the crust on a Great Basin–wide scale, may be informative for a wide range of topics and processes beyond the scope of this study. For example, correlation of tuff deposits and linking individual tuffs to source calderas has been challenging in some cases due to large tuff volumes, widespread distributions due to paleotopography, and varying levels of exposure and concealment by sedimentary basins. Our new data are consistent with the hypothesized location of the tuff of Cove Mine caldera ~20 km to the north and between the Fish Creek Mountains and the Caetano Tuff calderas (Fig. 1; Henry and John, 2013), as it is on-trend and intermediate to the Fish Creek Mountains and Caetano Tuff in the O-Sr longitudinal profile (Fig. 3). Recent mapping, geochemistry, petrography, and geochronology indicate that the Nine Hill caldera is within the northern part of the Elevenmile Canyon caldera in the Stillwater caldera complex (Fig. 2), in contrast to previous interpretations for its source caldera beneath the Carson Sink to the west of the Stillwater Range (Best et al., 1989; Henry and John, 2013). Our new oxygen and strontium isotope data for Nine Hill place it isotopically between the Campbell Creek and Fairview Peak calderas (Fig. 3), and thus are consistent with new mapping and interpretations.

O-Sr longitudinal trends also bear on hypothesized links between crustal structure and metallogeny in the Great Basin. For example, middle Cenozoic Carlin-type gold deposits, which cumulatively form the second largest concentration of gold on Earth, may have had gold and other metals derived from Proterozoic sediments of the miogeocline in central and eastern Nevada (Vikre et al., 2011). Because the middle Cenozoic caldera-forming tuffs track miogeoclinal sedimentary components in their source magmas, they offer important constraints for testing metallogenesis models. Two very large (>465 metric tons) Carlin-type gold deposits (Cortez and Cortez Hills) are located along the northeastern margin of the Caetano caldera in central Nevada (cf. Watts et al., 2016). The Caetano Tuff has the largest miogeoclinal sedimentary contribution of the 16 calderas studied (Fig. 3), and therefore these isotopic parameters may be useful for delineating favorable areas for Carlin-type mineralization.

Sources of High-, Normal-, and Low-$\delta^{18}O$ Crustal Components in the First Caldera Cycle of the Stillwater Caldera Complex

The first caldera cycle in the Stillwater caldera complex, ca. 29 Ma Job Canyon, produced high-, normal-, and low-$\delta^{18}O$ magmas, and, therefore, there must have been normal- to high-$\delta^{18}O$ and low-$\delta^{18}O$ crustal components over relatively restricted spatial scales at the onset of Stillwater magmatism. Inherited zircons in Job Canyon cycle rocks are broadly reflective of major flare-up events in the Mesozoic (Fig. 4). Late Cretaceous (76–71 Ma and 97–95 Ma) grains dominate the inherited zircon populations and overlap the ages of the three Stillwater basement plutons and the oxygen isotopic composition of zircons from the Sand Springs pluton (Fig. 4A). Inherited ages also overlap with two of the Late Cretaceous granitic plutons in the vicinity (New York Canyon and Rocky Canyon) that were found to have similar whole-rock $\delta^{18}O$ and $^{87}Sr/^{86}Sr_i$ compositions to normal- to high-$\delta^{18}O$ Stillwater magmas (Figs. 3–4). In contrast, the La Plata Canyon and Alameda Canyon plutons have $\delta^{18}O$ values that are higher, and the Sand Springs pluton has $\delta^{18}O$ values that overlap normal- to high-$\delta^{18}O$ Job Canyon magmas, but $^{87}Sr/^{86}Sr_i$ ratios that are lower (Fig. 3). A few older grains in the pre–Job Canyon dacite tuff, including Middle–Late Jurassic (166–150 Ma) and Neoproterozoic (545 Ma), increase the diversity of the inherited zircons. The 150 Ma grain has an oxygen isotopic composition that is identical within error to the Late Cretaceous inherited grains and the Sand Springs pluton zircons (Fig. 4A, inset). Therefore, it appears that a variety of normal- to high-$\delta^{18}O$ crustal components could have contributed to the initial oxygen isotope signatures of Stillwater magmas (probably most similar to the New York Canyon stock, based on combined $\delta^{18}O$ and $^{87}Sr/^{86}Sr_i$), but the source of the low-$\delta^{18}O$ component is unclear. The absence of low-$\delta^{18}O$ zircons in any of the investigated Mesozoic granitic plutons (this study; King et al., 2004; Blum et al., 2016) indicates that whatever the low-$\delta^{18}O$ source, it was not tapped during previous episodes of crustal melting.

Here, we evaluate potential rock reservoirs that could have been altered by meteoric waters to yield a low-$\delta^{18}O$ crustal component in the first low-$\delta^{18}O$ caldera-forming tuff of the Stillwater complex, the tuff of Job Canyon (see next discussion section for evaluation of the Poco Canyon and Elevenmile Canyon cycles). Stillwater calderas overlie three distinct Mesozoic basement terranes (Sand Springs, Quartz Mountain, and Jungo) that consist of clastic, volcanic, and carbonate rocks that were accreted to the continental margin, metamorphosed, and intruded by Jurassic and Cretaceous plutons (Fig. 9; cf. Crafford, 2007, 2008; Vetz, 2011; Vikre, 2014). Reasonable initial sources for a low-$\delta^{18}O$ crustal component could be the Middle Jurassic Humboldt mafic complex or the Early Triassic Koipato Group rocks, as they both have extensive exposures of hydrothermally altered rocks to the north of the Stillwater caldera complex (Kistler and Speed, 2000; Johnson, 2000; Vikre, 2014), and they are projected beneath or within the basement terranes that host the Stillwater complex (Fig. 9). Each of these could have been thrust-thickened and transported downward, potentially ~7–14 km, during crustal shortening associated with the Jurassic Luning-Fencemaker fold-and-thrust events (Wyld et al., 2003). Despite these facts, the isotopic data and age inheritance observed in the Stillwater caldera complex are not consistent with either of these potential sources. The Humboldt mafic complex has $^{87}Sr/^{86}Sr_i$ of 0.7041–0.7043, and the Koipato Group has $^{87}Sr/^{86}Sr_i$ of 0.709–0.712 (Kistler and Speed, 2000; Vetz, 2011), which are vastly different from magmas of the Stillwater caldera complex, which have $^{87}Sr/^{86}Sr_i$ of 0.7049–0.7057. The age of the Humboldt mafic complex is close to overlapping with one inherited grain found in the pre–Job Canyon dacite tuff, whereas no inherited grains correspond to the age of the Koipato Group rocks. Local Cretaceous granitic plutons are also commonly hydrothermally altered, some with mineralization (Wilden and Speed, 1974; Johnson et al., 1986; Quade and Tingley, 1987). Though none of the Cretaceous plutons in the immediate vicinity is an isotopic match in $\delta^{18}O$ and $^{87}Sr/^{86}Sr_i$ for Stillwater magmas, the New York Canyon stock and Rocky Canyon pluton to the north are very similar. Perhaps most importantly, zircon inheritance in the Job Canyon cycle is dominated by Cretaceous grains. Therefore, Job Canyon cycle magmas unequivocally traveled through and incorporated Cretaceous crust.

Potential depths of partial melting and assimilation of hydrothermally altered Cretaceous plutons into the Job Canyon magma chamber must be considered in this hypothesis. Unlike the hydrothermally altered Triassic–Jurassic basement rocks, which may have been transported downward during the Jurassic Luning-Fencemaker fold-and-thrust events, no syn– or post–Late Cretaceous episodes of crustal shortening occurred in this part of Nevada to transport altered Cretaceous plutons to deeper crustal levels. The Sevier orogeny peaked during the Late Cretaceous, but the front of this fold-and-thrust belt was much farther east in the Great Basin and would not have resulted in crustal shortening in basement rocks beneath the Stillwater caldera complex in western Nevada (cf. Dickinson, 2006). Notwithstanding this issue, granitic plutons can be altered by meteoric waters to significant depths. For example, the lowest exposed parts of the IXL pluton (~10 km paleodepth) in the Job Canyon caldera have highly altered whole-rock $\delta^{18}O$ values of ~0‰ (Fig. 10).

Because assimilation would have happened at shallow depths in the crust, thermal constraints must also be considered. Pre–Job Canyon andesite eruptions indicate that mafic magmas were heating the crustal block prior to the formation of the tuff of Job Canyon magma chamber. These andesites are some of the earliest preserved evidence of slab roll-back magmatism in the Stillwater region. Decompression of the asthenosphere during slab roll-back is presumed to have led to the formation of large volumes of basaltic magmas that perturbed the local geothermal gradient and promoted large-scale crustal melting (cf. Best et al., 2016). No basalts erupted in or around the Stillwater caldera complex at its inception ca. 30–29 Ma, but basaltic andesites (54–58 wt% SiO_2) erupted peripherally to the Stillwater complex from ca. 34 to 32 Ma near the Fairview Peak caldera and West Gate (~0–25 km south) and near the Deep Canyon caldera and Edwards Creek Valley (~5–20 km northeast). The presence of mafic enclaves (56–58 wt% SiO_2) in the IXL pluton (John, 1995) provides direct evidence for basaltic andesite in the shallow crust beneath Stillwater calderas.

The spatial extent and depth of midcrustal sills, crustal melt zones, or other salient features are unresolvable by geophysics due to late Cenozoic extension and magmatism that have profoundly modified the structure of the crust in the Great Basin. Geophysical imaging of the Altiplano-Puna volcanic complex, which is perhaps the closest modern-day analogue to the Great Basin ignimbrite flare-up (Best et al., 2016), reveals a composite partial melt zone that is continuous from depths of ~4 to 25 km (Ward et al., 2014), and modeling of the thermal structure of the crust indicates a temperature of ~500 °C at ~10 km depth (Gottsmann et al., 2017). Numerical thermodynamic modeling for low-$\delta^{18}O$ rhyolites in the Snake River Plain, which are comparable in volume to the tuff of Job Canyon (>55 km^3), have shown that basaltic sills can generate superheated silicic magmas that melt and assimilate ~20%–50% of even relatively cold (400 °C) country rocks to form low-$\delta^{18}O$ rhyolites (Simakin and Bindeman, 2012). Additional thermomechanical models by Colón et al. (2018) highlighted the importance of rheological discontinuities in the upper crust to focus melting. Heterogeneous distributions of Cretaceous plutonic rocks beneath the Stillwater caldera

complex may have been the source of such discontinuities that aided the melting process.

Model of Low-$\delta^{18}O$ Rhyolite Genesis in the Stillwater Caldera Complex

The appearance of a large-volume, low-$\delta^{18}O$ rhyolite during the first caldera cycle diverges from the caldera "cannibalization" paradigm, in which younger calderas are expected to exhibit $\delta^{18}O$ depletions through time as a result of remelting or "cannibalizing" hydrothermally altered parts of older calderas with which they overlap (e.g., Bindeman and Valley, 2001; Bindeman et al., 2008; Watts et al., 2011, 2012). However, other aspects of the oxygen isotope evolution of the Stillwater caldera complex are strikingly similar to the caldera cannibalization model, most notably, the extreme isotopic diversity of zircons within and between caldera cycles (Fig. 5). All caldera cycles have units with low-$\delta^{18}O$ zircons (<4.5‰), but only the Poco Canyon caldera cycle has units that are dominated by low-$\delta^{18}O$ zircons. The appearance of the low-$\delta^{18}O$ tuff of Poco Canyon after the first Job Canyon caldera cycle, and the potential spatial overlap of its caldera with the

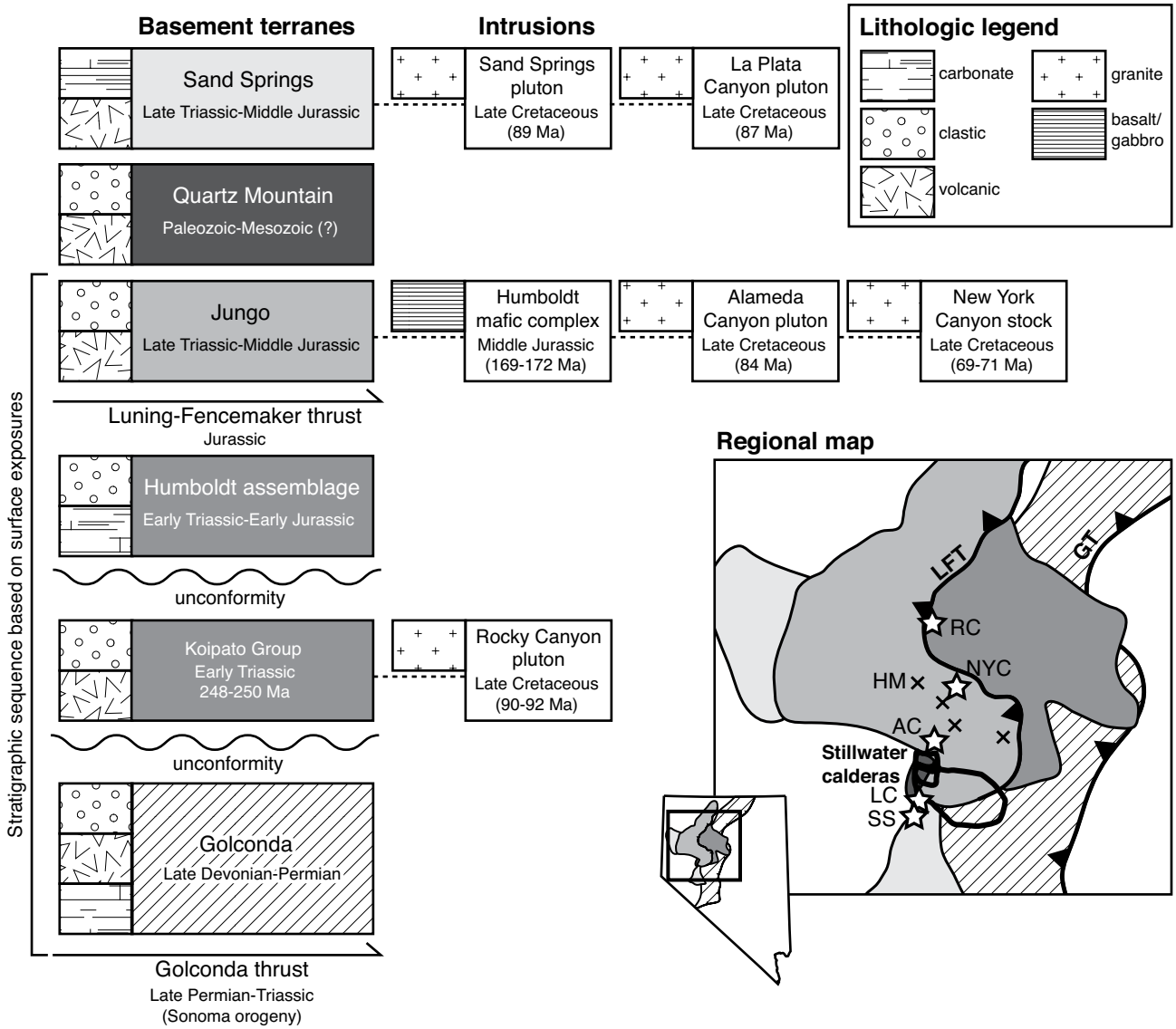

Figure 9. Relative stratigraphic positions and lithologic characteristics of Mesozoic basement terranes and intrusions projected beneath the Stillwater caldera complex in western Nevada. The Stillwater caldera complex is located at the intersection of the Sand Springs, Quartz Mountain, and Jungo terranes. The Jungo terrane is thrust over the Humboldt assemblage by the Luning-Fencemaker thrust (LFT) and is unconformably underlain by the Koipato Group volcanic rocks, which in turn are unconformably underlain by the Golconda terrane and the Golconda thrust (GT) (cf. Crafford, 2007, 2008; Vetz, 2011; Wyld et al., 2003; Dickinson, 2006). Note that the Koipato Group rocks are part of the Humboldt assemblage (Crafford, 2007). Stars in the inset map show the locations of granitic intrusions (SS—Sand Springs; LC—La Plata Canyon; AC—Alameda Canyon; NYC—New York Canyon; RC—Rocky Canyon); crosses show outcrops of the Humboldt mafic complex (HM).

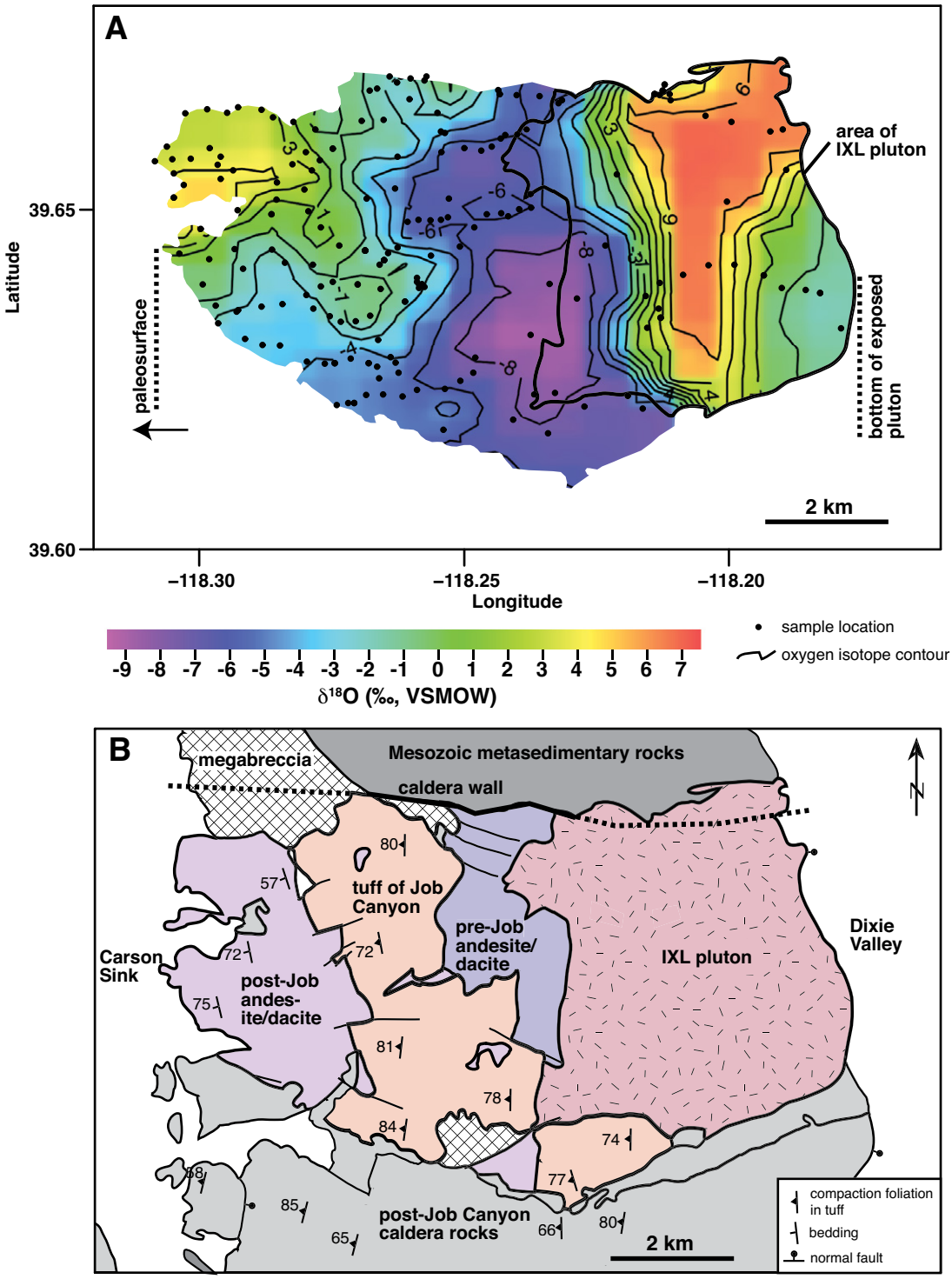

Figure 10. Contoured oxygen isotope data for (A) hydrothermally altered rocks in the Job Canyon caldera, with (B) individual units and features labeled. Whole-rock oxygen isotope data from John and Pickthorn (1996) were contoured using Aabel geochemical plotting software. In panel (A), sample locations are shown by the black dots, and the area of the IXL pluton is outlined in a heavy black line. The caldera is tilted to nearly vertical, with the paleosurface to the west and the bottom of the exposed pluton to the east.

Job Canyon caldera (Fig. 2; John, 1995; Colgan et al., 2018) present the possibility that its genesis was related to cannibalization of hydrothermally altered rocks from the Job Canyon cycle. Note that although the low-$\delta^{18}O$ tuff of Job Canyon was produced during the first caldera cycle, most magmas of that cycle were normal- to high-$\delta^{18}O$, including the last large-volume manifestation of silicic magmatism, the IXL pluton with unimodal $\delta^{18}O_{zircon}$ of 6.2‰–6.3‰. This evidence supports derivation of Job Canyon cycle magmas from isotopically diverse crust, with rare pockets of low-$\delta^{18}O$ material, perhaps altered Cretaceous plutons, as described in the previous section. In contrast, the low-$\delta^{18}O$ source of the tuff of Poco Canyon was continuous enough that all parts of the tuff and the precaldera rhyolite of Coyote Canyon have nearly unimodal $\delta^{18}O_{zircon}$ of 4.0‰–4.3‰ (Fig. 5C). Unlike the Job Canyon cycle, which possessed many inherited zircon grains, only one inherited zircon (98 Ma) was documented in the Poco Canyon cycle (Fig. 4A).

To test whether Job Canyon caldera rocks are feasible protoliths for the low-$\delta^{18}O$ tuff of Poco Canyon, Sr-O isotopic mass balance models were constructed (Figs. 10–11; Table 3). Whole-rock $\delta^{18}O$ data for a comprehensive suite of hydrothermally altered Job Canyon caldera rocks over an ~10 km paleodepth range (>200 analyses; John and Pickthorn, 1996) were contoured to approximately proportional areas of $\delta^{18}O$ values (Fig. 10). We note that the meteoric-hydrothermal system is characterized by near-neutral pH assemblages (K-feldspar stable propylitic, illitic, and intermediate argillic assemblages) that decrease in intensity up section, with an earlier phase of acid alteration (sericitic and advanced argillic) that is present locally at the top of the tuff and associated with postcaldera andesite dikes. Integrated $\delta^{18}O_{whole\text{-}rock}$ averages over depth profiles from ~6 to 10 km, ~5 to 10 km, and ~4 to 10 km are of 0.9‰, –1.5‰, and –2.0‰, respectively (Table 3). Assuming a normal-$\delta^{18}O$ starting magma with 7.5‰, estimated from normal-$\delta^{18}O$ zircons in the tuff of Poco Canyon and normal-$\delta^{18}O$ Stillwater magmas, and modeled for the full range of initial $^{87}Sr/^{86}Sr$ values (0.7049–0.7057) in the Stillwater caldera complex (Fig. 11; Table 3), the results indicate ~20% mass contribution from the Job Canyon intracaldera block using the ~4–10 km depth (6 km thickness) and ~5–10 km depth (5 km thickness) sections or ~30% using the ~6–10 km depth (4 km thickness; IXL pluton only).

Volume estimates of the tuff of Poco Canyon (~250–500 km^3) and the Job Canyon intracaldera block over the defined ~4–10 km depth range (~80–480 km^3) were then used to calculate the percentage of the Job Canyon intracaldera block volume in the tuff of Poco Canyon (Table 4). For intermediate volumes for the tuff of Poco Canyon (375 km^3) and Job Canyon intracaldera block (250 km^3), the required percentage of the Job Canyon intracaldera block volume is ~30% (Table 4). The lowest required percentage is ~10%, assuming a maximum Job Canyon intracaldera block volume and a minimum tuff of Poco Canyon volume (Table 4). Conversely, the highest required percentage is >100%, if using a minimum Job Canyon intracaldera block volume and a maximum tuff of Poco Canyon volume (Table 4). The mostly feasible results indicate that the hypothesis for cannibalized Job Canyon components in the

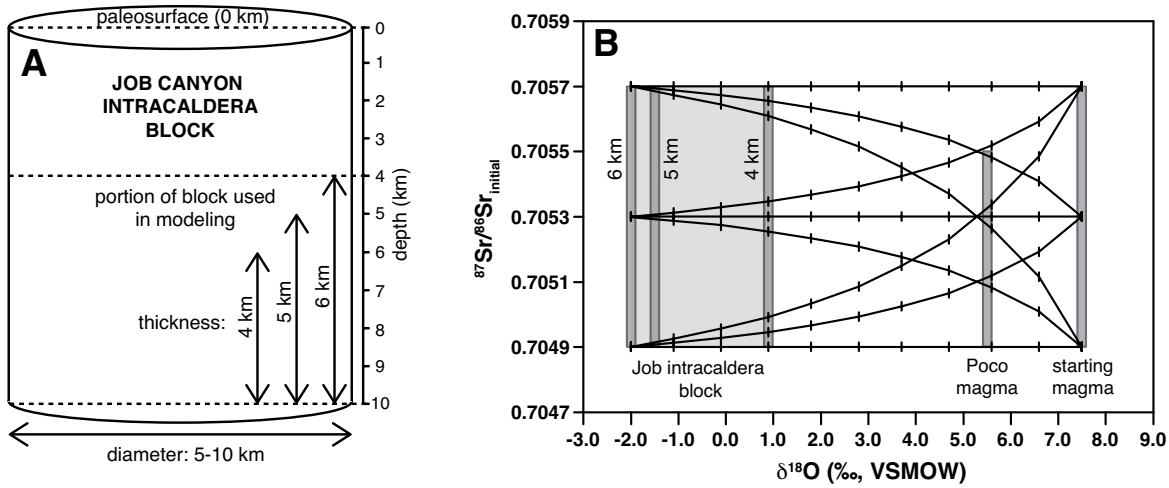

Figure 11. Modeling of the Job Canyon intracaldera block as a component in the low-$\delta^{18}O$ tuff of Poco Canyon magma. (A) Schematic representation of the Job Canyon intracaldera block as a cylinder with a diameter of 5–10 km and a thickness of 4–6 km (4–10 km paleodepth range). (B) Sr-O isotopic mixing models constructed between a hypothetical normal-$\delta^{18}O$ starting magma and the low-$\delta^{18}O$ Job intracaldera block; nine curves are modeled for high (0.7057), intermediate (0.7053), and low (0.7049) $^{87}Sr/^{86}Sr_i$ values. Isotopic mixing curves were calculated with the following equation for a two component system: $R_{mix} = [R_A C_A F_A + R_B C_B (1 - F_A)]/[C_A F_A + C_B (1 - F_A)]$, where R_{mix} is the isotopic ratio of the mixed magma composition, R is the isotope ratio for each element, C is the element concentration, F is the mass fraction, and components A and B represent the starting magma and the Job Canyon intracaldera block assimilant; tick marks demarcate 10% increments. Starting magma parameters were estimated from the least-evolved tuff of Poco Canyon samples and high-$\delta^{18}O$ zircons in the tuff of Poco Canyon (150 ppm Sr, 0.7049–0.7057 $^{87}Sr/^{86}Sr_i$, 48.57 wt% O, $\delta^{18}O$ = 7.5‰). Job Canyon intracaldera block assimilant parameters were estimated from the average of the IXL pluton, pre–Job Canyon andesite-dacite, and tuff of Job Canyon samples (500 ppm Sr, 0.7049–0.7057 $^{87}Sr/^{86}Sr_i$, 47.87 wt% O, $\delta^{18}O$ = 0.9‰ to –2.0‰). See Tables 3–4 for additional details.

TABLE 3. PARAMETERS AND CALCULATIONS OF LOW-$\delta^{18}O$ JOB CANYON INTRACALDERA BLOCK PERCENTAGE IN THE TUFF OF POCO CANYON

Depth of Job Canyon intracaldera block below paleosurface	Area (km^2)	Thickness (km)	Volume* (km^3)	$\delta^{18}O$ average† (‰)	% in Poco magma§ (%)
~6–10 km (IXL pluton only)	24	4	80–320	0.9	30
~5–10 km (IXL pluton + ~1 km of pre–Job andesite/dacite and tuff of Job Canyon rocks)	34	5	100–400	–1.5	20
~4–10 km (IXL pluton + ~2 km of pre–Job andesite/dacite and tuff of Job Canyon rocks)	40	6	120–480	–2.0	20

*Calculated as a cylinder, with r = 2.5–5 km (based on 5–10 km diameter of the Job Canyon caldera) and h = 4–6 km thickness.
†Approximated from proportional areas and $\delta^{18}O$ values in the Job Canyon caldera $\delta^{18}O$ contour map (Fig. 10).
§Sr-O isotopic mixing model percentage of Job Canyon intracaldera block assimilant (Fig. 11).

low-$\delta^{18}O$ Poco Canyon magma is viable. The required volume could be substantially lower if (1) the starting magma had a $\delta^{18}O$ composition lower than 7.5‰, (2) the low-$\delta^{18}O$ assimilated part of the Job Canyon block was more depleted than the –2.0‰ average, or (3) the volume of the Job Canyon block was close to or exceeding the upper bounds of the estimated volume range. For example, if the starting magma was 7.0‰, the assimilant was –6‰, and the volume of the Job Canyon block was at the upper modeled bound, ~4% of its total volume would be required.

We highlight a few critical observations to consider in alternative models of low-$\delta^{18}O$ rhyolite genesis. First, no inherited Job Canyon zircons were found in the tuff of Poco Canyon. Because the Job Canyon zircons are ca. 29 Ma in age, their presence in the ca. 25 Ma Poco Canyon magma should have been apparent, unless they were completely dissolved (we note that errors on individual $^{206}Pb/^{238}U$ ages of Stillwater zircons range from ~0.2 to 2.5 m.y., average of 0.3–0.5 m.y.). In this study, we did document one inherited grain in the tuff of Poco Canyon (98 Ma), which overlaps inherited grains in the Job Canyon cycle (Fig. 4A). We cannot rule out the possibility that the tuff of Poco Canyon also tapped a hydrothermally altered Cretaceous crustal source, as advocated for the tuff of Job Canyon. However, as described above, the low-$\delta^{18}O$ zircon record in the Poco Canyon cycle is clearly disparate from the Job Canyon cycle, and the paucity of inherited Mesozoic or Job Canyon grains in the Poco Canyon cycle is a problem for either hypothesis. Second, field evidence for partial melting of intracaldera Job Canyon rocks is lacking; for example, obvious melt lenses or dikes through the IXL pluton have not been found despite detailed mapping. Although we have a nearly complete ~10 km vertical section through the Job Canyon caldera, it is a single slice of a three-dimensional caldera. The volume of the intracaldera block that is modeled to be involved in the cannibalization process is <30% and could be <5%–10% if using less conservative model parameters; statistically, it is likely to be represented in other parts of the three-dimensional caldera that are not exposed in the single vertical slice. Third, another possible low-$\delta^{18}O$ crustal source in the tuff of Poco Canyon, if not Mesozoic basement or Job Canyon cycle rocks, may be older Oligocene calderas that underlie the Stillwater caldera complex. The ca. 30.4 Ma Deep Canyon caldera is exposed ~25 km to the east of the Job Canyon and Poco Canyon calderas (Fig. 2). Perhaps other calderas like it beneath the Poco Canyon caldera could have contributed low-$\delta^{18}O$ source rocks. The lack of xenocrysts makes all of these possibilities difficult to assess.

Though the tuff of Elevenmile Canyon was not a nominally low-$\delta^{18}O$ rhyolite, it has a remarkably diverse zircon record that is instructive for low-$\delta^{18}O$ rhyolite genesis models. Multimodal $\delta^{18}O$ spectra characterize zircons from all samples of the tuff of Elevenmile Canyon across the ~60 km caldera (Figs. 2 and 5D). Zircon cores and interiors are highly heterogeneous ($\delta^{18}O_{zircon}$ of ~4‰–8‰), whereas zircon rims have a homogenized value ($\delta^{18}O_{zircon}$ of ~6‰) (Fig. 6B). Two low-$\delta^{18}O$ zircons (<4.5‰) for which we also have trace element data indicate that they are an identical match to zircons from the tuff of Poco Canyon, with the distinctive negative Eu anomalies in REE patterns (Figs. 7E–7F). The tuff of Louderback Mountains is another potential source of the low-$\delta^{18}O$ zircons, based on our published trace element data (Colgan et al., 2018). This evidence indicates that the tuff of Elevenmile Canyon magma chamber may have cannibalized Poco Canyon and/or Louderback Mountains components in the parts of its magma chamber that overlapped these calderas. The pattern apparent in the tuff of Elevenmile Canyon, with isotopically diverse zircon cores overgrown by homogenized rims that approximate the bulk zircon average (Fig. 6), is remarkably similar to observations for the large-volume, low-$\delta^{18}O$ Kilgore Tuff of the Heise volcanic field in the eastern Snake River Plain (Watts et al., 2011), and supports our view that large silicic magma chambers are assembled from isotopically diverse batches of melt in the shallow crust.

Finally, aspects of the regional caldera centers to which we extended our oxygen isotopic

TABLE 4. MODEL RESULTS FOR PERCENTAGE OF LOW-$\delta^{18}O$ JOB CANYON INTRACALDERA BLOCK VOLUME IN THE TUFF OF POCO CANYON

~6–10 km depth (IXL pluton only); $\delta^{18}O$ = 0.9‰

Tuff of Poco Canyon		total IXL pluton volume (km^3)		
Volume (km^3)	30% volume (km^3)	80	200	320
		% of IXL pluton volume required		
250	75	*94*	37	23
375	113	*162*	*56*	35
500	150	*187*	*75*	47

~5–10 km depth (IXL pluton + pre–Job andesite/dacite + tuff of Job Canyon); $\delta^{18}O$ = –1.5‰

Tuff of Poco Canyon		total ~5–10 km depth volume (km^3)		
Volume (km^3)	20% volume (km^3)	100	250	400
		% of ~5–10 km depth volume required		
250	50	50	20	12
375	75	*75*	30	19
500	100	*100*	40	25

~4–10 km depth (IXL pluton + pre–Job andesite/dacite + tuff of Job Canyon); $\delta^{18}O$ = –2.0‰

Tuff of Poco Canyon		total ~4–10 km depth volume (km^3)		
Volume (km^3)	20% volume (km^3)	120	300	480
		% of ~4–10 km depth volume required		
250	50	42	17	10
375	75	*62*	25	16
500	100	*83*	33	21

Note: Italics indicate >50% volume (considered an unrealistic model result).

investigation are pertinent to low-$\delta^{18}O$ rhyolite genesis models. It is instructive that in addition to the Stillwater caldera complex, the Mount Jefferson caldera complex exhibits a clear depletion in $\delta^{18}O$ through time. Quartz in the upper tuff of Mount Jefferson is ~1‰ lower than the lower tuff of Mount Jefferson (Fig. 3A), supporting a model in which low-$\delta^{18}O$ crust was assimilated into the upper tuff of Mount Jefferson magma chamber. In addition, the Manhattan caldera, which may overlap the mineralized Round Mountain caldera, is distinctly lower in $\delta^{18}O$ compared to other tuffs in the area, and may have assimilated altered parts of the Round Mountain caldera or perhaps altered Cretaceous granites in the vicinity (Henry and John, 2013). In contrast, the nested calderas studied by Larson and Taylor (1986) in the central Nevada volcanic field produced high-$\delta^{18}O$ magmas with a subtle ~0.4‰ depletion from the early to middle eruptive sequence and a return to the initial higher values in the late eruptive sequence. These authors did not have the benefit of high-spatial-resolution zircon data; their interpretations may have underestimated contributions from isotopically diverse crustal components. Nonetheless, the nested calderas studied by Larson and Taylor (1986) are ~75–100 km east of the paleodivide boundaries defined by Henry and John (2013) and Best et al. (2013a) (Fig. 1). Therefore, these calderas formed on the Nevadaplano topographic crest in the middle Cenozoic (e.g., DeCelles, 2004). By analogue with the Altiplano region of the Central Andes, it may be that the lack of low-$\delta^{18}O$ rhyolites in this part of Nevada was due to a lack of meteoric water in a high-elevation, arid environment (Folkes et al., 2013). Interestingly, the caldera-forming tuffs studied by Larson and Taylor (1986) in the central Nevada volcanic field have ages of ca. 32–24 Ma (Best et al., 2013b), which overlap those of the Stillwater caldera complex. Located well to the west of the paleodivide boundary, the Stillwater complex may have been better positioned for the establishment of caldera lakes and other surface-water features to promote hydrothermal circulation and alteration of shallow crustal rocks.

Relationship between Caldera-Forming Tuffs and Granitic Plutons in the Stillwater Caldera Complex

All investigated cycles of the Stillwater caldera complex have pluton or porphyry systems that are spatially coincident with calderas (Fig. 2; Colgan et al., 2018). Despite this spatial association, our new oxygen isotope data are clearly disparate for tuff and pluton samples for all caldera cycles except the tuff of Elevenmile Canyon, in which six analyzed samples of the tuff are very similar to the granodiorite phase of the Freeman Creek pluton (Fig. 5D). Trace element data collected for the same zircons analyzed for oxygen isotopes provide further support of this observation; only the tuff of Elevenmile Canyon and Freeman Creek pluton granodiorite have identical $\delta^{18}O$, Hf, and REE patterns (Fig. 7). The IXL pluton has discernibly younger zircon U-Pb ages than the tuff of Job Canyon (28.5–28.1 Ma for IXL pluton and 29.2 Ma for the tuff of Job Canyon), but U-Pb ages for all other spatially associated tuffs and plutons are indistinguishable within error (Table 2). It is clear that relying on field evidence and geochronology alone to assess volcanic-plutonic relationships is insufficient in the Stillwater caldera complex, and highlights the necessity of crystal-scale chemical and isotopic data to make robust conclusions about these processes in the Great Basin and worldwide. Our findings for the Stillwater caldera complex indicate that, in general, caldera-forming tuffs and plutons are not derived from the same magmatic sources. This is in direct contrast to our previous finding for the well-exposed 34.0 Ma Caetano caldera in north-central Nevada, where a cogenetic relationship between the caldera-forming tuff and large caldera intrusions is unequivocal based on many lines of whole-rock and crystal-scale evidence (Watts et al., 2016). We highlight that none of the plutonic or porphyry units appears to have assimilated low-$\delta^{18}O$ crust, and we speculate that this may be due to a lower-temperature, waning phase of silicic magmatism that did not favor digestion of shallow crustal materials.

CONCLUSIONS

Voluminous silicic tuffs (>3000–5000 km^3) of the Stillwater caldera complex possess a remarkably diverse oxygen isotopic record. All caldera cycles have low-$\delta^{18}O$ zircons, providing unequivocal evidence for recycling of hydrothermally altered crust in the formation and growth of silicic magma chambers that yielded climactic caldera-forming eruptions. Both existing hydrothermally altered crust from Mesozoic plutons, and cannibalization of hydrothermally altered intracaldera rocks in overlapping calderas, were likely important in generating low-$\delta^{18}O$ rhyolites in the Stillwater caldera complex (Fig. 12). The low-$\delta^{18}O$ tuffs of Job Canyon and Poco Canyon have a combined volume of >400 km^3 and are the first documented low-$\delta^{18}O$ rhyolites in middle Cenozoic calderas of the Great Basin, extending the geographic distribution of these isotopically distinctive and important magma types. The 2500–5000 km^3 tuff of Elevenmile Canyon is one of the most voluminous tuffs produced during the Great Basin ignimbrite flare-up, and has a zircon record that points to rapid batch assembly of isotopically diverse melts in the upper crust, possibly including components from previous caldera cycles, and thus it is instructive for low-$\delta^{18}O$ rhyolite genesis models, even though it is not a nominally low-$\delta^{18}O$ rhyolite. We emphasize the importance of analyzing nominally normal-$\delta^{18}O$ rhyolites with high-spatial-resolution methods, as processes associated with crustal recycling are likely to be obscure in the Great Basin and other regions with high-$\delta^{18}O$ (meta) sedimentary contributions to magmas. We note that none of the single (isolated) calderas in our regional study produced low-$\delta^{18}O$ rhyolites, but that the nested Mount Jefferson calderas exhibit $\delta^{18}O$ depletions through time, and that the Manhattan caldera, which may also be nested, has a distinctly lower $\delta^{18}O$ signature than other calderas in the region. This evidence supports a model in which overlapping calderas facilitate the generation of low-$\delta^{18}O$ rhyolites. Nested calderas of the Stillwater complex exhibit a high level of diversity in space and time. Despite spatial and temporal overlap of calderas, each caldera-forming eruption has a unique isotopic fingerprint that is apparent from single zircon analyses. Furthermore, spatially associated plutons that intrude calderas are in most cases not genetically equivalent to the caldera-forming tuffs. Our work in the Great Basin has implications for caldera-related processes globally, particularly for mechanisms of shallow crustal recycling, which can be an important component in magmatism that produces hazardous eruptions from caldera volcanoes, but one that is not commonly identified. More isotopic studies are required to assess their global occurrence and significance.

ACKNOWLEDGMENTS

Aki Ishida and Noriko Kita are thanked for providing guidance during preparation and use of the WiscSIMS ion microprobe, and Kim Klaussen is thanked for her assistance in data collection. Peter Vikre and Steve Ludington provided helpful conversations about the regional basement geology in western Nevada. We thank Brian Cousens for performing strontium isotope analyses at Carleton University and for sharing his graduate student Kim's time to travel and participate in analytical work at the WiscSIMS laboratory. The following individuals are thanked for their guidance during analytical sessions: Jim Palandri at the University of Oregon Stable Isotope Laboratory, Jorge Vazquez and Matt Coble at the Stanford–USGS SHRIMP-RG laboratory, and Leslie O'Brien at the USGS Menlo Park microanalytical facility. We acknowledge Mark Stelten, Henrietta Cathey, and an anonymous reviewer for their careful reviews and

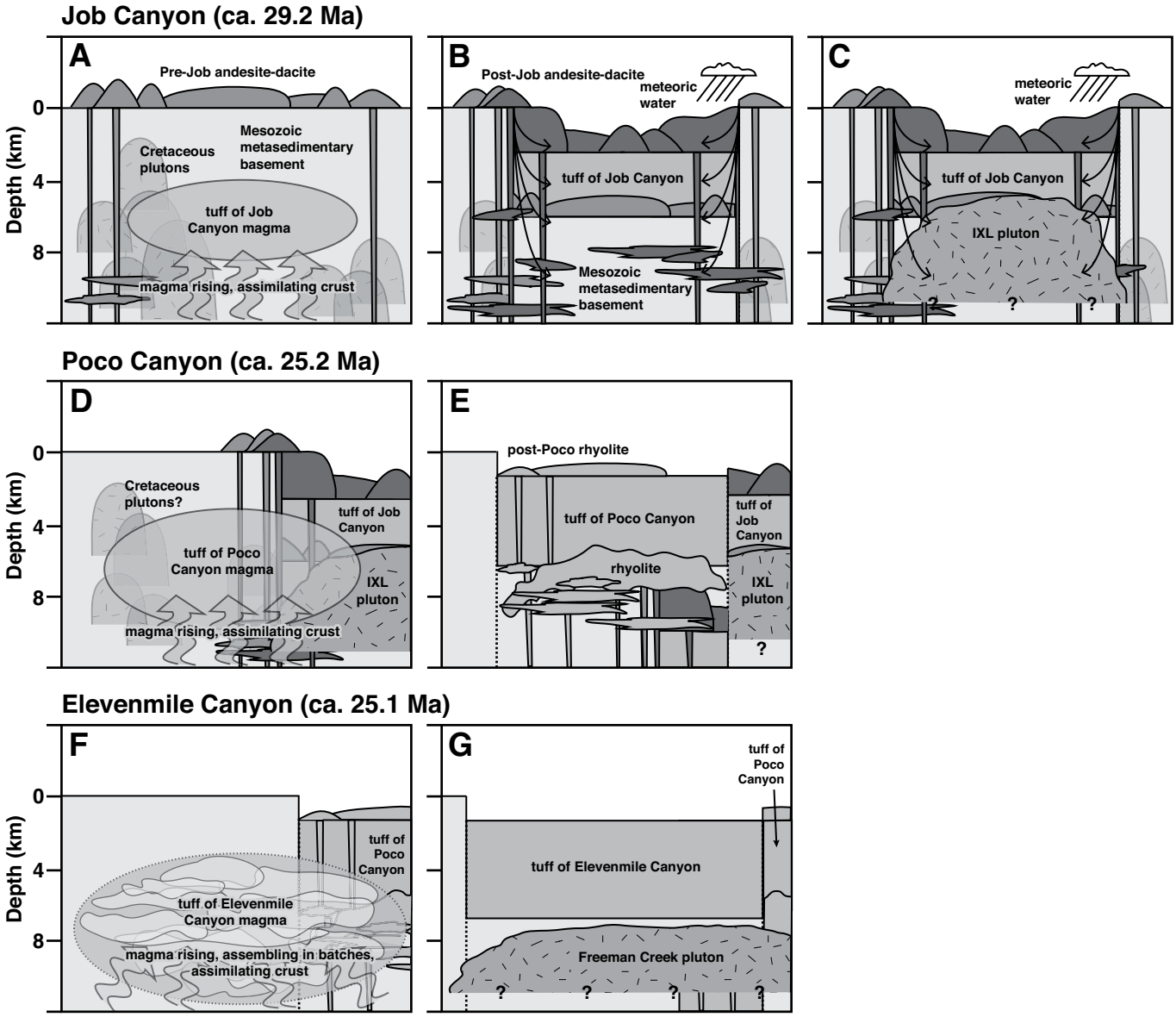

Figure 12. Schematic synthesis of petrogenetic processes in the Stillwater caldera complex. (A) Pre–Job Canyon andesite-dacite lavas and small-volume tuffs with zircon inheritance from Mesozoic basement crust, probably dominated by Cretaceous plutons. The tuff of Job Canyon magma chamber may have assimilated hydrothermally altered Cretaceous plutons to attain its low-$\delta^{18}O$ signature. (B) Caldera-forming tuff of Job Canyon fills the Job Canyon caldera. It is represented over a thickness of ~2 km, but it is faulted and not a uniform thickness as shown in the schematic figure. Post–Job Canyon andesite-dacite lavas tap isotopically heterogeneous crust. Meteoric water penetrates the caldera. (C) IXL pluton intrudes the Job Canyon caldera. A large convective hydrothermal system driven by heat from the IXL pluton and dominated by meteoric water alters the intracaldera block, including parts of the pluton. (D) The tuff of Poco Canyon magma chamber partially overlapped the Job Canyon caldera and may have assimilated some of the hydrothermally altered Job Canyon intracaldera block. It may also have assimilated altered Cretaceous plutons. (E) Caldera-forming eruption of the tuff of Poco Canyon fills the Poco Canyon caldera. It is represented over a thickness of ~4.5 km, but it is faulted and not a uniform thickness as shown in the schematic figure. The tuff is underlain and overlain by rhyolite lava flows and intrusions. (F) Tuff of Elevenmile Canyon magmas are assembled as isotopically diverse batches that attain a homogenized value over time. The tuff of Elevenmile Canyon magma chamber overlaps the Poco Canyon caldera and may have assimilated some of the intracaldera Poco Canyon block. (G) Caldera-forming eruption of the tuff of Elevenmile Canyon is one of the largest in the Great Basin. Intracaldera tuff fills the caldera basin to a thickness of ~5 km. The composite Freeman Creek pluton intrudes rocks beneath the level of exposure of the tuff. The tuff is possibly cogenetic with the granodiorite phase of the Freeman Creek pluton. The granite phase of the Freeman Creek pluton intrudes the granodiorite phase and the composite pluton underlies both the Elevenmile Canyon and Poco Canyon calderas.

guidance in improving the manuscript. This research was supported by the USGS National Cooperative Geologic Mapping Program, Mineral Resources Program, and Mendenhall Research Fellowship Program. WiscSIMS is supported by the National Science Foundation (EAR-1355580, EAR-1658823) and the University of Wisconsin–Madison. Valley is supported by the U.S. Department of Energy (DOE), Office of Basic Energy Sciences, Geosciences Division (DE-FG02-93ER14389). Any use of trade, firm, or product names is for descriptive purposes only and does not imply endorsement by the U.S. government.

REFERENCES CITED

Ankney, M.E., Bacon, C.R., Valley, J.W., Beard, B.L., and Johnson, C.M., 2017, Oxygen and U-Th isotopes and the timescales of hydrothermal exchange and melting in granitoid wall rocks at Mount Mazama, Crater Lake, Oregon: Geochimica et Cosmochimica Acta, v. 213, p. 137–154, https://doi.org/10.1016/j.gca.2017.04.043.

Bacon, C.R., Adami, L.H., and Lanphere, M.A., 1989, Direct evidence for the origin of low ^{18}O silicic magmas: Quenched samples of a magma chamber's partially-fused granitoid walls, Crater Lake, Oregon: Earth and Planetary Science Letters, v. 96, p. 199–208, https://doi.org/10.1016/0012-821X(89)90132-5.

Barth, A.P., and Wooden, J.L., 2010, Coupled elemental and isotopic analyses of polygenetic zircons from granitic rocks by ion microprobe, with implications for melt evolution and the sources of granitic magmas: Chemical Geology, v. 277, p. 149–159, https://doi.org/10.1016/j.chemgeo.2010.07.017.

Barton, M.D., 1990, Cretaceous magmatism, metamorphism, and metallogeny in the east-central Great Basin, *in* Anderson, J.L., ed., The Nature and Origin of Cordilleran Magmatism: Geological Society of America Memoir 174, p. 283–302, https://doi.org/10.1130/MEM174-p283.

Best, M.G., Christiansen, E.H., Deino, A.L., Gromme, C.S., McKee, E.H., and Noble, D.C., 1989, Eocene through Miocene volcanism in the Great Basin of the western United States, *in* Chapin, C.E., and Zidek, J., eds., Field Excursions to Volcanic Terranes in the Western United States, Volume II: Cascades and Intermountain West: New Mexico Bureau of Mines and Mineral Resources Memoir 47, p. 91–133.

Best, M.G., Christiansen, E.H., and Gromme, S., 2013a, Introduction: The 36–18 Ma southern Great Basin, USA, ignimbrite province and flareup: Swarms of subduction-related supervolcanoes: Geosphere, v. 9, p. 260–274, https://doi.org/10.1130/GES00870.1.

Best, M.G., Gromme, C.S., Deino, A.L., Christiansen, E.H., and Tingey, D.G., 2013b, The 36–18 Ma Central Nevada ignimbrite field and calderas, Great Basin, USA: Multicyclic super-eruptions: Geosphere, v. 9, p. 1562–1636, https://doi.org/10.1130/GES00945.1.

Best, M.G., Christiansen, E.H., Deino, A.L., Gromme, S., Hart, G.L., and Tingey, D.G., 2013c, The 36–18 Ma Indian Peak–Caliente ignimbrite field and calderas, southeastern Great Basin, USA: Multicyclic super-eruptions: Geosphere, v. 9, p. 864–950, https://doi.org/10.1130/GES00902.1.

Best, M.G., Christiansen, E.H., de Silva, S., and Lipman, P., 2016, Slab-rollback ignimbrite flareups in the southern Great Basin and other Cenozoic American arcs: A distinct style of arc volcanism: Geosphere, v. 12, p. 1097–1135, https://doi.org/10.1130/GES01285.1.

Bindeman, I.N., 2008, Oxygen isotopes in mantle and crustal magmas as revealed by single crystal analysis, *in* Putirka, K.D., and Tepley, F.J., eds., Minerals, Inclusions and Volcanic Processes: Reviews in Mineralogy and Geochemistry, v. 69, p. 445–478, https://doi.org/10.2138/rmg.2008.69.12.

Bindeman, I.N., and Valley, J.W., 2001, Low-$\delta^{18}O$ rhyolites from Yellowstone: Magmatic evolution based on analyses of zircons and individual phenocrysts: Journal of Petrology, v. 42, p. 1491–1517, https://doi.org/10.1093/petrology/42.8.1491.

Bindeman, I.N., and Valley, J.W., 2003, Rapid generation of both high- and low-$\delta^{18}O$, large-volume silicic magmas at the Timber Mountain/Oasis Valley caldera complex, Nevada: Geological Society of America Bulletin, v. 115, p. 581–595, https://doi.org/10.1130/0016-7606(2003)115<0581:RGOBHA>2.0.CO;2.

Bindeman, I.N., Ponomareva, V.V., Bailey, J.C., and Valley, J.W., 2004, Volcanic arc of Kamchatka: A province with high-$\delta^{18}O$ magma sources and large-scale $^{18}O/^{16}O$ depletion of the upper crust: Geochimica et Cosmochimica Acta, v. 68, p. 841–865, https://doi.org/10.1016/j.gca.2003.07.009.

Bindeman, I.N., Fu, B., Kita, N., and Valley, J.W., 2008, Origin and evolution of Yellowstone silicic magmatism based on ion microprobe analysis of isotopically-zoned zircons: Journal of Petrology, v. 49, p. 163–193, https://doi.org/10.1093/petrology/egm075.

Bindeman, I.N., Gurenko, A., Carley, T., Miller, C., Martin, E., and Sigmarsson, O., 2012, Silicic magma petrogenesis in Iceland by remelting of hydrothermally altered crust based on oxygen isotope diversity and disequilibria between zircon and magma with implications for MORB: Terra Nova, v. 24, p. 227–232, https://doi.org/10.1111/j.1365-3121.2012.01058.x.

Black, L.P., Kamo, S.L., Allen, C.M., Davis, D.W., Aleinikoff, J.N., Valley, J.W., Mundil, R., Campbell, I.H., Korsch, R.J., Williams, I.S., and Foudoulis, C., 2004, Improved $^{206}Pb/^{238}U$ microprobe geochronology by the monitoring of a trace-element–related matrix effect; SHRIMP, ID-TIMS, ELA-ICP-MS and oxygen isotope documentation for a series of zircon standards: Chemical Geology, v. 205, p. 115–140, https://doi.org/10.1016/j.chemgeo.2004.01.003.

Blum, T.B., Kitajima, K., Nakashima, D., Strickland, A., Spicuzza, M.J., and Valley, J.W., 2016, Oxygen isotope evolution of the Lake Owyhee volcanic field, Oregon, and implications for the low-$\delta^{18}O$ magmatism of the Snake River Plain–Yellowstone hotspot and other low-$\delta^{18}O$ large igneous provinces: Contributions to Mineralogy and Petrology, v. 171, article 92, https://doi.org/10.1007/s00410-016-1297-x.

Boroughs, S.B., Wolff, J., Bonnichsen, B., Godchaux, M., and Larson, P., 2005, Large volume, low-$\delta^{18}O$ rhyolites of the central Snake River Plain, Idaho, USA: Geology, v. 33, p. 821–824, https://doi.org/10.1130/G21723.1.

Colgan, J.P., John, D.A., Henry, C.D., and Fleck, R.J., 2008, Large-magnitude extension of the Eocene Caetano caldera, Shoshone and Toiyabe Ranges, Nevada: Geosphere, v. 4, p. 107–130, https://doi.org/10.1130/GES00115.1.

Colgan, J.P., John, D.A., Henry, C.D., and Watts, K.E., 2018, Insights into the emplacement of upper-crustal plutons and their relationship to large silicic calderas, from field relationships, geochronology, and zircon trace element geochemistry in the Stillwater–Clan Alpine caldera complex, western Nevada, USA: Journal of Volcanology and Geothermal Research, v. 349, p. 163–176, https://doi.org/10.1016/j.jvolgeores.2017.10.015.

Colón, D.P., Bindeman, I.N., Ellis, B.S., Schmitt, A.K., and Fisher, C.M., 2015, Hydrothermal alteration and melting of the crust during the Columbia River Basalt–Snake River Plain transition and the origin of low-$\delta^{18}O$ rhyolites of the central Snake River Plain: Lithos, v. 224–225, p. 310–323, https://doi.org/10.1016/j.lithos.2015.02.022.

Colón, D.P., Bindeman, I.N., and Gerya, T.V., 2018, Thermomechanical modeling of the formation of a multilevel, crustal-scale magmatic system by the Yellowstone plume: Geophysical Research Letters, v. 45, p. 3873–3879, https://doi.org/10.1029/2018GL077090.

Coney, P.J., 1978, Mesozoic–Cenozoic Cordilleran plate tectonics, *in* Smith, R.B., and Eaton, G.P., eds., Cenozoic Tectonics and Regional Geophysics of the Western Cordillera: Geological Society of America Memoir 152, p. 33–50, https://doi.org/10.1130/MEM152-p33.

Coney, P.J., and Reynolds, S.J., 1977, Cordilleran Benioff zones: Nature, v. 270, p. 403–406, https://doi.org/10.1038/270403a0.

Crafford, A.E.J., 2007, Geologic Map of Nevada: U.S. Geological Survey Data Series 249, scale 1:250,000, 1 CD-ROM, 46 p., 1 plate, http://pubs.usgs.gov/ ds/2007/249/.

Crafford, A.E.J., 2008, Paleozoic tectonic domains of Nevada: An interpretive discussion to accompany the geologic map of Nevada: Geosphere, v. 4, p. 260–291, https://doi.org/10.1130/GES00108.1.

DeCelles, 2004, Late Jurassic to Eocene evolution of the Cordilleran thrust belt and foreland basin system, western USA: American Journal of Science, v. 304, p. 104–168.

Dickinson, W.R., 2006, Geotectonic evolution of the Great Basin: Geosphere, v. 2, p. 353–368, https://doi.org/10.1130/GES00054.1.

Drew, D.L., Bindeman, I.N., Watts, K.E., Schmitt, A.K., Fu, B., and McCurry, M., 2013, Crustal-scale recycling in caldera complexes and rift zones along the Yellowstone hotspot track: O and Hf isotopic evidence in diverse zircons from voluminous rhyolites of the Picabo volcanic field, Idaho: Earth and Planetary Science Letters, v. 381, p. 63–77, https://doi.org/10.1016/j.epsl.2013.08.007.

Ellis, B.S., Barry, T., Branney, M.J., Wolff, J.A., Bindeman, I., Wilson, R., and Bonnichsen, B., 2010, Petrologic constraints on the development of a large-volume, high-temperature, silicic magma system: The Twin Falls eruptive centre, central Snake River Plain: Lithos, v. 120, p. 475–489, https://doi.org/10.1016/j.lithos.2010.09.008.

Farmer, G.L., and DePaolo, D.J., 1983, Origin of Mesozoic and Tertiary granite in the western United States and implications for pre-Mesozoic crustal structure: 1. Nd and Sr isotopic studies in the geocline of the northern Great Basin: Journal of Geophysical Research, v. 88, p. 3379–3401, https://doi.org/10.1029/JB088iB04p03379.

Folkes, C.B., de Silva, S.L., Bindeman, I.N., and Cas, R.A.F., 2013, Tectonic and climate history influence the geochemistry of large-volume silicic magmas: New $\delta^{18}O$ data from the Central Andes with comparison to N. America and Kamchatka: Journal of Volcanology and Geothermal Research, v. 262, p. 90–103, https://doi.org/10.1016/j.jvolgeores.2013.05.014.

Gottsmann, J., Blundy, J., Henderson, S., Pritchard, M.E., and Sparks, R.S.J., 2017, Thermomechanical modeling of the Altiplano-Puna deformation anomaly: Multiparameter insights into magma mush reorganization: Geosphere, v. 13, p. 1042–1065, https://doi.org/10.1130/GES01420.1.

Grunder, A.L., 1987, Low $\delta^{18}O$ silicic volcanic rocks at the Calabazos caldera complex, Southern Andes: Contributions to Mineralogy and Petrology, v. 95, p. 71–81, https://doi.org/10.1007/BF00518031.

Harris, C., and Erlank, A.J., 1992, The production of large-volume, low-$\delta^{18}O$ rhyolites during the rifting of Africa and Antarctica: The Lebombo monocline, southern Africa: Geochimica et Cosmochimica Acta, v. 56, p. 3561–3570, https://doi.org/10.1016/0016-7037(92)90399-4.

Henry, C.D., and John, D.A., 2013, Magmatism, ash-flow tuffs, and calderas of the ignimbrite flareup in the western Nevada volcanic field, Great Basin, USA: Geosphere, v. 9, p. 951–1008, https://doi.org/10.1130/GES00867.1.

Hildreth, W., Christiansen, R.L., and O'Neil, J.R., 1984, Catastrophic isotopic modification of rhyolitic magma at times of caldera subsidence, Yellowstone Plateau volcanic field: Journal of Geophysical Research, v. 89, p. 8339–8369, https://doi.org/10.1029/JB089iB10p08339.

Humphreys, E.D., 1995, Post-Laramide removal of the Farallon slab, western United States: Geology, v. 23, p. 987–990, https://doi.org/10.1130/0091-7613(1995)023<0987:PLROTF>2.3.CO;2.

John, D.A., 1995, Tilted mid-Cenozoic ash-flow calderas and subjacent granitic plutons, southern Stillwater Range, Nevada: Cross-sections of an Oligocene igneous center: Geological Society of America Bulletin, v. 107, p. 180–200, https://doi.org/10.1130/0016-7606(1995)107<0180:TMTAFC>2.3.CO;2.

John, D.A., and Pickthorn, W.J., 1996, Alteration and stable isotope studies of a deep meteoric-hydrothermal system in the Job Canyon caldera and IXL pluton, southern Stillwater Range, Nevada, *in* Coyner, A.R., and Fahey, P.L., eds., Geology and Ore Deposits of the American Cordillera: Reno/Sparks, Nevada, Geological Society of Nevada, Symposium Proceedings, April 1995, p. 733–756.

John, D.A., Henry, C.D., and Colgan, J.P., 2008, Magmatic and tectonic evolution of the Caetano caldera,

north-central Nevada: A tilted, mid-Tertiary eruptive center and source of the Caetano Tuff: Geosphere, v. 4, p. 75–106, https://doi.org/10.1130/GES00116.1.

Johnson, D.A., 2000, Comparative Studies of Iron-Oxide Mineralization: Great Basin [Ph.D. dissertation]: Tucson, Arizona, University of Arizona, 451 p.

Johnson, K.M., Ludington, S.D., and Gray, K., 1986, A peraluminous, tungsten-mineralized stock at New York Canyon, Pershing County, Nevada: Geological Society of America Abstracts with Programs, v. 18, p. 122.

Johnson, M.G., 1977, Geology and mineral deposits of Pershing County, Nevada: Nevada Bureau of Mines and Geology Bulletin 89, 121 p.

King, E.M., Valley, J.W., Stockli, D.F., and Wright, J.E., 2004, Oxygen isotopic trends of granitic magmatism in the Great Basin: Location of the Precambrian craton boundary as reflected in zircons: Geological Society of America Bulletin, v. 116, p. 451–462, https://doi.org/10.1130/B25324.1.

Kistler, R.W., and Speed, R.C., 2000, $^{40}Ar/^{39}Ar$, K-Ar, Rb-Sr Whole-Rock and Mineral Ages, Chemical Composition, Strontium, Oxygen and Hydrogen Isotopic Systematics of Jurassic Humboldt Lopolith and Permian (?) and Triassic Koipato Group Rocks, Pershing and Churchill Counties, Nevada: U.S. Geological Survey Open-File Report 00-217, 14 p., https://doi.org/10.3133/ofr00217.

Kita, N.T., Ushikubo, T., Fu, B., and Valley, J.W., 2009, High precision SIMS oxygen isotope analyses and the effect of sample topography: Chemical Geology, v. 264, p. 43–57, https://doi.org/10.1016/j.chemgeo.2009.02.012.

Lackey, J.S., Valley, J.W., Chen, J.H., and Stockli, D.F., 2008, Dynamic magma systems, crustal recycling, and alteration in the central Sierra Nevada batholith: The oxygen isotope record: Journal of Petrology, v. 49, p. 1397–1426, https://doi.org/10.1093/petrology/egn030.

Larson, P.B., and Taylor, H.P., 1986, $^{18}O/^{16}O$ ratios in ash-flow tuffs and lavas erupted from the central Nevada caldera complex and the central San Juan caldera complex, Colorado: Contributions to Mineralogy and Petrology, v. 92, p. 146–156, https://doi.org/10.1007/BF00375290.

Loewen, M.W., and Bindeman, I.N., 2015, Oxygen isotope and trace element evidence for three-stage petrogenesis of the youngest episode (260–79 ka) of Yellowstone rhyolitic volcanism: Contributions to Mineralogy and Petrology, v. 170, p. 39, https://doi.org/10.1007/s00410-015-1189-5.

Ludwig, K.R., 2012, Isoplot 3.75, A geochronological toolkit for Excel: Berkeley Geochronology Center Special Publication 5, 75 p.

Miller, C.F., and Wark, D.A., 2008, Supervolcanoes: Elements, v. 4, p. 11–15, https://doi.org/10.2113/GSELEMENTS.4.1.11.

Mutch, E.J.F., Blundy, J.D., Tattich, B.C., Cooper, F.J., and Brooker, R.A., 2016, An experimental study of amphibole stability in low-pressure granitic magmas and a revised Al-in-hornblende geobarometer: Contributions to Mineralogy and Petrology, v. 171, p. 85, https://doi.org/10.1007/s00410-016-1298-9.

Pope, E.C., Bird, D.K., and Arnórsson, S., 2013, Evolution of low-^{18}O Icelandic crust: Earth and Planetary Science Letters, v. 374, p. 47–59, https://doi.org/10.1016/j.epsl.2013.04.043.

Putirka, K., 2016, Amphibole thermometers and barometers for igneous systems and some implications for eruption mechanisms of felsic magmas at arc volcanoes: The American Mineralogist, v. 101, p. 841–858, https://doi.org/10.2138/am-2016-5506.

Quade, J., and Tingley, J.V., 1987, Mineral resource inventory, U.S. Navy master land withdrawal area, Churchill County, Nevada: Nevada Bureau of Mines and Geology Open-File Report 87-2, 99 p.

Ridolfi, F., Renzulli, A., and Puerini, M., 2010, Stability and chemical equilibrium of amphibole in calc-alkaline magmas: An overview, new thermobarometric formulations and application to subduction-related volcanoes: Contributions to Mineralogy and Petrology, v. 160, p. 45–66, https://doi.org/10.1007/s00410-009-0465-7.

Seligman, A., Bindeman, I., Jicha, B., Ellis, B., Ponomareva, V., and Leonov, V., 2014, Multi-cyclic and isotopically diverse silicic magma generation in an arc volcano: Gorely eruptive center, Kamchatka, Russia: Journal of Petrology, v. 55, p. 1561–1594, https://doi.org/10.1093/petrology/egu034.

Simakin, A.G., and Bindeman, I.N., 2012, Remelting in caldera and rift environments and the genesis of hot, "recycled" rhyolites: Earth and Planetary Science Letters, v. 337–338, p. 224–235, https://doi.org/10.1016/j.epsl.2012.04.011.

Solomon, G.C., and Taylor, H.P., Jr., 1989, Isotopic evidence for the origin of Mesozoic and Cenozoic granitic plutons in the northern Great Basin: Geology, v. 17, p. 591–594, https://doi.org/10.1130/0091-7613(1989)017<0591:IEFTOO>2.3.CO;2.

Stepner, D.A., 2017, Source and Magma Evolution of the Tuff of Elevenmile Canyon, Stillwater Range, Clan Alpine and Northern Desatoya Mountains, Western Nevada [M.S. thesis]: Ottawa, Ontario, Canada, University of Ottawa, 166 p.

Taylor, H.P., 1986, Igneous rocks II. Isotopic case studies of circum-Pacific magmatism: Reviews in Mineralogy and Geochemistry, v. 16, p. 273–316.

Trail, D., Bindeman, I.N., Watson, E.B., and Schmitt, A.K., 2009, Experimental calibration of oxygen isotope fractionation between quartz and zircon: Geochimica et Cosmochimica Acta, v. 73, p. 7110–7126, https://doi.org/10.1016/j.gca.2009.08.024.

Troch, J., Ellis, B.S., Mark, D.F., Bindeman, I.N., Kent, A.J., Guillong, M., and Bachmann, O., 2017, Rhyolite generation prior to a Yellowstone supereruption: Insights from the Island Park–Mount Jackson rhyolite series: Journal of Petrology, v. 58, p. 29–52.

Valley, J.W., 2003, Oxygen isotopes in zircon, *in* Hanchar, J.M., and Hoskin, P.W.O., eds., Zircon: Review in Mineralogy and Geochemistry, v. 53, p. 343–385.

Valley, J.W., and Kita, N.T., 2009, In situ oxygen isotope geochemistry by ion microprobe, *in* Fayek, M., ed., Mineralogical Association of Canada Short Course 41: Secondary Ion Mass Spectrometry in the Earth Sciences, p. 19–63.

Valley, J.W., Bindeman, I.N., and Peck, W.H., 2003, Empirical calibration of oxygen isotope fractionation in zircon: Geochimica et Cosmochimica Acta, v. 67, p. 3257–3266, https://doi.org/10.1016/S0016-7037(03)00090-5.

Varve, S., 2013, Stratigraphy, Geochemistry, and Origin of the Fish Creek Mountains Tuff, Battle Mountain Area, North-Central Nevada, USA [M.S. thesis]: Ottawa, Ontario, Canada, Carleton University, 141 p.

Vetz, N.Q., 2011, Geochronologic and Isotopic Investigation of the Koipato Formation, Northwestern Great Basin, Nevada: Implications for Late Permian–Early Triassic Tectonics along the Western U.S. cordillera [M.S. thesis]: Boise, Idaho, Boise State University, 147 p.

Vikre, P., 2014, Magmatism, metasomatism, tectonism and mineralization in the Humboldt Range, Pershing County, Nevada: Geological Society of Nevada Field Trip Guidebook to the Humboldt Range: Reno, Nevada, Geological Society of Nevada, 14 p.

Vikre, P.G., Poulson, S.R., and Koenig, A.E., 2011, Derivation of S and Pb in Phanerozoic intrusion-related metal deposits from Neoproterozoic sedimentary pyrite, Great Basin, United States: Economic Geology and the Bulletin of the Society of Economic Geologists, v. 106, p. 883–912, https://doi.org/10.2113/econgeo.106.5.883.

Wang, X.-L., Coble, M.A., Valley, J.W., Shu, X.-J., Kitajima, K., Spicuzza, M.J., and Sun, T., 2014, Influence of radiation damage on Late Jurassic zircon from southern China: Evidence from in situ measurement of oxygen isotopes, laser Raman, U-Pb ages, and trace elements: Chemical Geology, v. 389, p. 122–136, https://doi.org/10.1016/j.chemgeo.2014.09.013.

Ward, K.M., Zandt, G., Beck, S.L., Christensen, D.H., and McFarlin, H., 2014, Seismic imaging of the magmatic underpinnings beneath the Altiplano-Puna volcanic complex from the joint inversion of surface wave dispersion and receiver functions: Earth and Planetary Science Letters, v. 404, p. 43–53, https://doi.org/10.1016/j.epsl.2014.07.022.

Watts, K.E., Bindeman, I.N., and Schmitt, A.K., 2011, Large-volume rhyolite genesis in caldera complexes of the Snake River Plain: Insights from the Kilgore Tuff of the Heise volcanic field, Idaho, with comparison to Yellowstone and Bruneau Jarbidge rhyolites: Journal of Petrology, v. 52, p. 857–890, https://doi.org/10.1093/petrology/egr005.

Watts, K.E., Bindeman, I.N., and Schmitt, A.K., 2012, Crystal-scale anatomy of a dying supervolcano: An isotope and geochronology study of individual phenocrysts from voluminous rhyolites of the Yellowstone caldera: Contributions to Mineralogy and Petrology, v. 164, p. 45–67, https://doi.org/10.1007/s00410-012-0724-x.

Watts, K.E., John, D.A., Colgan, J.P., Henry, C.D., Bindeman, I.N., and Schmitt, A.K., 2016, Probing the volcanic-plutonic connection and the genesis of crystal-rich rhyolite in a deeply dissected supervolcano in the Nevada Great Basin: Source of the late Eocene Caetano Tuff: Journal of Petrology, v. 57, p. 1599–1644, https://doi.org/10.1093/petrology/egw051.

Wilden, R., and Speed, R.C., 1974, Geology and Mineral Deposits of Churchill County, Nevada: Nevada Bureau of Mines and Geology Bulletin 83, 103 p.

Wooden, J.L., Kistler, R.W., and Tosdal, R.M., 1999, Strontium, Lead, and Oxygen Isotopic Data for Granitoid and Volcanic Rocks from the Northern Great Basin and Sierra Nevada, California, Nevada and Utah: U.S. Geological Survey Open-File Report 99–569, 20 p.

Wyld, S.J., Rogers, J.W., and Copeland, P., 2003, Metamorphic evolution of the Luning-Fencemaker fold-thrust belt, Nevada: Illite crystallinity, metamorphic petrology, and $^{40}Ar/^{39}Ar$ geochronology: The Journal of Geology, v. 111, p. 17–38, https://doi.org/10.1086/344663.

Science Editor: Aaron J. Cavosie
Associate Editor: Chloe Bonamici

Manuscript Received 27 April 2018
Revised Manuscript Received 6 September 2018
Manuscript Accepted 19 November 2018

Printed in the USA